Title: Effective hemostasis requires networks of oxidized lipids (eoxPL) in cell membranes that support calcium-dependent coagulation factor binding.

One sentence summary: Enzymatically-oxidized phospholipids from circulating blood cells and platelets support coagulation in vivo through increasing calcium-dependent association of clotting factors with membrane surfaces, and are elevated and immunogenic in human thrombotic disease.

Authors: Sarah N Lauder[1,2], *Keith Allen-Redpath[1,2], *David A Slatter[1,2], Maceler Aldrovandi[1,2], Anne O'Connor[1,2], Daniel Farewell[3], Charles L Percy[1,2], Jessica E Molhoek[4], Sirpa Rannikko[5], Victoria J Tyrrell[1,2], Salvatore Ferla[6], Ginger L Milne[7], Alastair W Poole[8], Christopher P Thomas[1,2,6], Samya Obaji[1,2], Philip R Taylor[1,2], Simon A Jones[1,2], Phillip G de Groot[4], Rolf T Urbanus[4], Sohvi Hörkkö[5], Stefan Uderhardt[9], Jochen Ackermann[9], P. Vince Jenkins[10], Andrea Brancale[6], Gerhard Krönke[9], Peter W Collins[1,2] and Valerie B O'Donnell[1,2].

Affiliations: [1]Systems Immunity Research Institute, [2]Institute of Infection & Immunity, [3]Division of Population Medicine, [6]Welsh School of Pharmacy and Pharmaceutical Sciences, Cardiff University, Heath Park, Cardiff, CF14 4XN, UK, [4]Department of Clinical Chemistry and Haematology, University of Utrecht, University Medical Center Utrecht, Utrecht, the Netherlands, [5]Department of Medical Microbiology and Immunology, Research Unit of Biomedicine, University of Oulu, Finland and Medical Research Center and Nordlab Oulu, University Hospital, Oulu, Finland, [7]Division of Clinical Pharmacology Vanderbilt University Medical Center, Nashville, Tennessee, USA, [8]School of Physiology, Pharmacy and Neuroscience, Medical Sciences Building, University Walk, Bristol BS8 1TD, [9]Department of Internal Medicine and Institute for Clinical Immunology, University Hospital Erlangen, Erlangen, Germany, [10]Institute of Molecular Medicine, St James's Hospital, Dublin, Ireland.

*These authors contributed jointly to the work.

Address Correspondence to:
Valerie O'Donnell (o-donnellvb@cardiff.ac.uk), or Peter Collins (collinspw@cardiff.ac.uk), Systems Immunity Research Institute, School of Medicine, Cardiff University, Heath Park, Cardiff, CF14 4XN, UK

Abstract

Coagulation is a critical event in innate immunity designed to prevent bacterial invasion and blood loss, that occurs on the external membrane surface of activated platelets and leukocytes. Herein, we show using lipidomic, genetic, biochemical and mathematical modeling approaches that enzymatically-oxidized phospholipids (eoxPL) from leukocyte or platelet lipoxygenases (LOX) are required for normal clotting, by promoting coagulation factor activities in a calcium and phosphatidylserine (PS)-dependent manner. In wild type mice, hydroxyeicosatetraenoic acid-phospholipids (HETE-PLs) enhanced coagulation, and restored normal hemostasis in p12- or 12/15-LOX deficient animals, which failed to generate normal thrombus in vivo. Murine platelets generated 22 diverse eoxPL species, that were missing in p12-LOX deficiency. Humans with the thrombotic disorder antiphospholipid syndrome (APS) had significantly elevated HETE-PLs in platelets and leukocytes, and higher HETE-PL immunoreactivity. HETE-PLs also enhanced membrane binding of β2GPI, a process considered central to developing an immune response in APS. Correlation network analysis of 47 platelet eoxPL species in APS and control platelets identified their enzymatic origin and revealed a complex network of regulation, with 31 p12-LOX-derived eoxPL significantly elevated in thrombotic disease. In summary, circulating blood cells generate networks of eoxPL, including HETE-PLs that change membrane properties to enhance clotting during innate immunity and bleeding challenge, and are significantly elevated in the thrombotic disease, APS.

Introduction

Blood clotting is an essential first step in innate immunity, required to prevent bacterial invasion and ensure effective hemostasis following injury. Excess clotting in the vasculature underlies vascular inflammatory conditions including myocardial infarction, stroke, pulmonary embolism and deep vein thrombosis, while impaired coagulation contributes to excessive blood loss during surgery and childbirth, the commonest cause of mortality during childbirth. Thus, a fuller understanding of the molecular processes underlying coagulation/hemostasis could drive development of effective new treatments and help inform prevention strategies for several major human disorders.

Hemostasis depends on the coagulation cascade, a series of serine proteases and co-factors in plasma, initiated by tissue factor (TF). For clotting to occur, amino-phospholipid (aPL) externalization on the platelet surface following activation is required. Here, scramblase leads to phosphatidylethanolamine (PE) and –serine (PS) translocation, providing a negative charge to facilitate calcium binding and factor association (1,2). aPL externalization alone is not sufficient for full physiological coagulation since the rare disorder Scott Syndrome presents with an inability to externalize PS/PE, but only a relatively minor bleeding phenotype, unless under significant haemostatic challenge (3). This suggests additional PLs are involved.

Activated platelets and leukocytes rapidly generate oxidized PEs and phosphatidylcholines (PCs) *via* lipoxygenases (LOX), termed hydroxyeicosatetraenoic acid-phospholipids (HETE-PL) that reside at or within the plasma membrane (4-10). HETE-PL positional isomers are exclusively cell type and LOX isoform dependent, thus 5-, 12- and 15-HETE-PLs are generated by human neutrophils, platelets or monocytes respectively. However, in mice, where leukocytes express a 12/15-LOX homolog, 12-

HETE-PLs are instead formed (7). We recently identified COX-1 derived enzymatically-oxidized PL (eoxPL) generated by platelets, containing either PGE_2, PGD_2 or dioxolane A3 (DXA_3), and then, using global lipidomics mass spectrometry mapped out 103 eoxPL molecular species in thrombin-activated human platelets (11-13). This indicated that eoxPL generation is a far broader phenomenon than previously thought, although the enzymatic origin of most members of this large group remained unknown.

Antiphospholipid syndrome (APS) is an acquired prothrombotic disorder caused by a diverse family of circulating "antiphospholipid" antibodies. These can be directed against phospholipids including PE or cardiolipin, β2GPI or other PL-binding proteins. In APS, pathogenic antibodies contribute to thrombotic episodes or pregnancy complications (14-16). An interaction between β2GPI and negatively-charged phospholipids on the surface of cells is thought to be required for disease development (15,16). The phospholipids that provide optimal binding of β2GPI to membranes are unknown. Given that eoxPL are generated at significant rates by isolated blood cells and platelets, contain electronegative hydroxyl groups on their fatty acids, and remain cell-associated after their formation, we decided to explore their generation in APS.

Herein, we use biochemical, genetic, clinical, mathematical and lipidomic approaches to reveal the pro-coagulant mechanisms of endogenously generated LOX-derived eoxPL from platelets and leukocytes in vitro and in vivo and show they increase β2GPI binding to membranes. We undertook correlation network analysis of the 47 most abundant eoxPL in platelets from a human APS cohort, revealing several levels of enzymatic regulation, and show their elevated generation and enhanced immune recognition in disease. Overall, our studies provide a novel paradigm for hemostasis where the generation of multiple eoxPL by platelets and leukocytes is required for normal

coagulation to occur, and is chronically elevated during human venous thrombotic disease associated with APS.

Results

HETE-PL isomers enhance thrombin generation in platelet poor plasma.

Coagulation requires multiple enzyme/cofactor complexes that ultimately generate thrombin (factor IIa, FIIa), specifically TF/FVIIa, FIXa/FVIIIa (intrinsic tenase) and FXa/FVa (prothrombinase), and takes place on phospholipid membranes (17-19). To support this, plasma membranes externalize aminophospholipids, PS and PE (17,18,20,21). It has been shown that PS is required to support coagulation whilst PE enhances PS activity (1,2,22). PS and PE bind coagulation factors II, VII, IX and X, in a calcium-dependent manner, through their gamma carboxylated glutamic acid (Gla) domains (17,23) and FVIII and FV through C domains (24,25). To examine the effects of HETE-PLs on coagulation, the lipids were incorporated into TF-containing liposomes and added to pooled plasma. Increasing concentrations of 5-,12- or 15-HETE-PE or –PC all enhanced coagulation in a concentration-dependent manner (Fig. 1 A to F).

HETE-PL enhance the prothrombotic action of PS in platelet poor plasma.

The accepted model of coagulation is that PS supports the prothrombinase and intrinsic tenase complexes, while PE enhances the effect of PS. PC is thought to have no role in supporting coagulation (2). To determine the pro-coagulant mechanisms of HETE-PLs, thrombin generation was measured at varying PS concentrations. In the absence of PS, native PE supported low thrombin generation, which doubled on substitution with 15-HETE-PE (Fig. 1, G and H). Gradually increasing PS led to dose dependent elevations in thrombin generation, which were similarly elevated by HETE-PE (Fig. 1, G and H). In contrast, PC (either native or HETE-PC) was unable to support thrombin generation without PE/PS (Fig. 1, I and J). Here, gradually increasing PS led to a dose dependent increase in thrombin generation. However, in contrast to HETE-PE, the enhancing effect

of HETE-PC was greater at higher PS concentrations (Fig. 1J). Specifically at 1 % or 30 % PS, HETE-PC increased thrombin generation approximately 20%, or 175%, respectively. This indicates a synergistic effect of HETE-PC with PS. The data indicate a mechanism by which HETE-PLs enhance PS dependent coagulation, similar to native PE, but far more potently. The pro-coagulant action of HETE-PC is highlighted since PC was previously assumed not to support PS in coagulation reactions (2,26).

HETE-PLs stimulate thrombin generation in a simplified, purified cascade. Thrombin generation in platelet poor plasma (PPP) is also influenced by anticoagulant factors. To further explore mechanisms, experiments were performed in a synthetic system using purified proteins at physiological concentrations of FII (1.4 μmol/L), FV (26 nmol/L), FVII (10 nmol/L), FVIII (300 pmol/L), FIX (80 nmol/L) and FX (136 nmol/L) without inhibitors of coagulation. Thrombin generation was triggered by TF-containing liposomes as for plasma experiments above. 15-, 12- and 5-HETE-PE and –PCs all significantly elevated thrombin generation (Fig. 1, K to M).

Molecular modeling shows bending of HETE with localization of –OH at the membrane surface, and association with calcium molecules. A molecular dynamics simulation was performed to understand how the hydroxyl group of 12-HETE-PC would behave within the membrane. An available pre-equilibrated DOPC membrane with 128 molecules was modified to give a composition of 5% SAPS, 5 % SAPC, 30% SAPE, 55% DOPC, 5% 12-HETE-PC. This includes 3 molecules of PS and HETE-PC per leaflet. On one side, HETE-PCs were placed with HETEs buried in the membrane (in the yellow hydrophobic compartment), while on the other they were placed in a bent up configuration, with the –OH close to the polar membrane surface. During the 300 ns simulation, the system

remained stable. The polar membrane surface is shown in blue, with uncharged PC headgroups in grey). Notably, during the simulation all of the HETE-PCs with HETEs pointing downwards changed conformation to place the -OH group at the charged surface of the membrane (blue), while those already in that configuration remained stable (Fig. 2, A to D). In this position the –OH could establish a hydrogen bond with the nearby lipid phosphates, and in some cases, with the carboxylic acid group of neighboring PS (Fig. 2D). The OH- also appeared to interact with calcium ions (Fig. 2, B and C). As expected, calcium ions (red) strongly interact with PS headgroups during the whole duration of the simulation (Fig. 2, C and D). As a result, both the HETE-OH and the PS carboxylic acid favor a close interaction between the surface of the membrane and the calcium ions of the water phase. We also visualized the bilayer from above (blue: positive charge, brown: negative charge) and note that the –OH is visible for all 3 HETE-PCs (red) facilitating formation of a more negatively charged space, pushing headgroups apart and making space for calcium to bind, in some cases near PS (pink) (Fig. 2E). A movie showing 12-HETE-PC movement during the 300 ns simulation is provided as supplementary (lipid simulation.avi). Viewing on a mac is best done with VLC Media Player (http://www.videolan.org/vlc/download-windows.en-GB.html). In this, the HETE was originally placed aligned to other fatty acyl groups but around 100 ns, it moves up to orientate the –OH group near the polar region, and remains there, near calcium for the remainder of the simulation.

HETE-PE increases calcium membrane binding. To experimentally test for an interaction of calcium with HETE-PLs, we measured Fluo-FF fluorescence in the presence of liposomes, maintaining PC, PS and total PE concentrations, but gradually replacing PE with 12-HETE-PE up to 10 %. In this assay, lipid-dependent lowering of Fluo-FF

fluorescence indicates elevated membrane calcium binding, which is then calculated as described in Methods. In the presence of either 10 or 20 μM $CaCl_2$, control liposomes bound 1 or 2.5 μM calcium, respectively. This increased significantly and almost doubled at 3 - 10 % HETE-PE (Fig. 2F). These data support our hypothesis that HETE-PLs facilitate calcium binding on the surface of membranes, to enhance PS-dependent clotting factor binding and activity.

HETE-PLs enhance coagulation and promote hemostasis in vivo. We next tested the ability of HETE-PLs to promote coagulation in vivo. For this, liposomes containing two different concentrations of 12-HETE-PE or PC were injected intradermally into the tails of wild type mice, immediately proximal to a tail cut. Control liposomes were without effect while either 78 or 19 ng HETE-PL (per injection) significantly inhibited bleeding, in some cases leading to total cessation (Fig. 3A). Separately, liposomes were injected i.v. into wild type mice and thrombin-antithrombin complexes (TAT) were significantly elevated after 1 hr where liposomes contained 19 ng 12-HETE-PE (Fig. 3B). These data indicate that HETE-PLs are pro-coagulant in healthy mice in vivo. Next, we measured eoxPL generation by murine platelets in vitro, from mice genetically lacking p12-LOX. Washed platelets from wild type but not p12-$LOX^{-/-}$ mice generated multiple isomers of 12-HETE-PE and –PC in response to thrombin activation (Fig. 3C, full data is shown in fig. S1). Both plasmalogen and acyl forms and also analogous eoxPL from 22:4, 22:5 and 22:6 fatty acids were found, with all requiring p12-LOX (Fig. 3C). Time courses showed that HETE-PLs are already elevated at 5 min but continued to increase at least to 30 min post thrombin activation (Fig. 3D).

Genetic deficiency of p12-LOX or 12/15-LOX leads to a bleeding defect that can be corrected with HETE-PE administration. To test the involvement of p12-LOX in regulating coagulation in vivo, venous thrombosis was induced using $FeCl_2$ as described in Methods. In humans, venous thrombosis is predominantly associated with dysregulated activation of coagulation factors, whereas platelet activation is associated with arterial thrombosis. In this model, significantly lower thrombus weight was observed in p12-LOX$^{-/-}$ mice (Fig. 4, A and B). Mice lacking either p12- or 12/15-LOX also showed a significantly increased tail bleeding time as well as elevated blood loss (Hb loss) (Fig. 4, C and D). We next tested whether administration of HETE-PLs restores hemostasis in vivo, in either p12- or 12/15-LOX$^{-/-}$ mice, by administering small doses immediately proximal to a tail cut. Control liposomes contain 65% PC, 35% PE and 5% PS and may be expected to have partial pro-coagulant activities depending on dose. In either case, administration of 19 ng 12-HETE-PE in liposomes restored hemostasis back to wild type amounts, and in all cases was significantly more effective than control liposomes at reducing bleeding time (Fig. 4, C and D). These data show that HETE-PLs are pro-coagulant in vivo, and our findings using LOX deficient strains provides an explanation why their absence in either platelets or leukocytes causes a bleeding defect.

Leukocyte and platelet HETE-PEs are elevated in APS. To characterize HETE-PL generation in a human disease associated with venous thrombosis, HETE-PEs were quantified in isolated platelets and leukocytes from patients with antiphospholipid syndrome and healthy controls. Basally, significantly elevated 5-HETE-PE (from neutrophils, monocytes, via 5-LOX) and 15-HETE-PE (from eosinophils, via 15-LOX) was detected in leukocytes from APS patients as compared to healthy volunteers (Fig. 5, A and B). Following calcium ionophore activation, HETE-PEs increased in both groups to a

similar amount (Fig. 5, A and B). This indicates that leukocyte LOXs generate HETE-PEs basally in APS. The lack of difference following ionophore stimulation between HC and APS could imply that 15- and 5-LOX expression is similar in leukocytes from both groups although HETE-PL generation will also depend on AA availability and re-esterification rate into lysoPLs. APS platelets contained significantly more 12-HETE-PE than controls, both basally and following thrombin activation (Fig. 5C). Furthermore, APS platelet isolates tended to spontaneously aggregate during isolation. Specifically, no healthy subject platelets aggregated until thrombin challenged, while of the 12 APS isolates, 9 appeared to at least slightly aggregate during the last washing step of platelet isolation, and of those, 7 generated a platelet "clot" that we removed and analyzed separately and show in Fig. 5 D. Our platelet isolation method is designed to minimize spontaneous activation. Thus, platelets from APS patients are inherently more "poised" to activate. The detailed reasons are unknown, but it is an important unanswered phenomenon in APS pathophysiology. 12-HETE-PE in these spontaneously-aggregated platelets was similar to amounts in thrombin-activated APS platelets (Fig. 5, C and D). Increased platelet activation in vivo in APS was confirmed by measuring 11-thromboxane B2 (TXB_2), a urinary metabolite of thromboxane A2 formed by platelet COX-1 (Fig. 5E). This is consistent with APS platelets circulating in a heightened activation state in vivo.

Next, we next analyzed leukocytes for platelet-derived 12-HETE-PEs and platelets for leukocyte-derived 5- and 15-HETE-PEs. 15- and 5-HETE-PEs were elevated basally in APS platelets (Fig. 5, F and G). Unlike 12-HETE-PE, these did not significantly increase with thrombin, indicating they were not from platelets, but could represent microparticles from other cells attached to platelets. APS leukocytes had elevated platelet 12-HETE-PE compared to controls, that increased further on ionophore activation (Fig. 5H). Thus, platelets or platelet-derived microparticles may be associated with APS

leukocytes during isolation and remain responsive to ionophore activation in vitro. It is well known that platelet derived microparticles are elevated in APS, and we previously showed that 12-HETE-PE and –PC can be present in vesicles generated by thrombin-activated platelets in vitro (9,27).

Our patients were almost all taking anti-coagulant medication thus an influence of this on eoxPL cannot be excluded (Supplementary Table 1). Although samples sizes were small, gender, age and concurrent arterial thrombosis did not appear to influence eoxPL levels (fig. S2).

APS patients have elevated plasma IgG directed against HETE-PEs.

We sought to determine if HETE-PLs act as an antigen for antibodies in APS by measuring HETE-PE-specific IgG, compared with the unoxidized analog, 1-stearoyl-2-arachidonyl-PE (SAPE). APS serum had a significant elevation in IgG recognizing 5-, 12- and 15-HETE-PEs (Fig. 6, A to C). IgG against SAPE was also increased, but this was not significant. Total IgG was comparable between groups (Fig. 6D). This suggests that chronic higher exposure to HETE-PEs leads to elevated immune recognition of these lipids in patients.

HETE-PEs enhance APS-associated plasma protein binding to the cellular surface.

β2GPI is a positively charged protein that binds to anionic PLs such as cardiolipin, resulting in a conformational change that exposes cryptic epitopes recognized by pathogenic disease-associated antibodies (15). This interaction is believed to result in downstream signaling with a net pro-coagulant effect. Since HETE-PLs can enhance calcium binding (Fig. 2F), we tested whether they can also increase β2GPI interactions with the plasma membrane using PS/PC containing-liposomes. Binding of human purified

β2GPI was enhanced by cardiolipin, or on substitution of SAPE with 15-HETE-PE (Fig. 6E). Also, 5- or 12-HETE-PE elevated cardiolipin-dependent β2GPI binding to the liposome in comparison to HETE-PEs or cardiolipin alone (Fig. 6F). Thus, HETE-PEs enhance binding of β2GPI to membranes, a process required for the protein to become antigenic.

Lipidomics defines the complexity of eoxPL enzymatic generation in human platelets including new control networks. Recently we showed that over 100 eoxPL are acutely generated by thrombin-activated human platelets (11-13). The enzymatic origin of most of these lipids was not defined. Here, the 47 most abundant were profiled in healthy control and APS platelets (both basally and after thrombin activation), to examine their behavior in the context of a thrombotic disease, and relative amounts are shown as a heatmap (Fig. 7A, full data including replicates is shown in fig. S3). In the heatmap, upregulation is denoted by red, and downregulation by blue. Deeper tones indicate greater differences, with comparisons made for individual lipids made across samples. Where origin is known, lipids were labeled as from either COX-1 (blue) or p12-LOX (red), based on either their absence in 12-LOX$^{-/-}$ mouse platelets, established herein, or for PGE_2- or DXA_3-PEs, a known sensitivity to aspirin (Fig. 3 D) (11,12). Clear clustering is seen with two prominent groups of related lipids visible based on COX-1 or p12-LOX. Several polyhydroxylated lipids grouped with COX-1 suggesting they may also originate from that pathway (green) while five mono-hydroxylipids (black) also grouped with p12-LOX. Notably, eoxPL clustered strongly based on the *Sn2* fatty acid, with HDOHEs, HETEs and monohydroxy C22 lipids forming associated groups. From visual inspection, 12-LOX derived lipids appear to upregulate stronger with thrombin than other lipids, and are higher in the APS vs HC groups.

Next, we plotted correlations between lipids (i.e. how each lipid behaves in relation to others individually) to further examine their behavior within the APS cohort (Fig. 7B). Here, lipids were sorted by decreasing correlation with 18:0a/12-HETE-PE, an abundant eoxPL generated by p12-LOX. As for the heatmap, p12-LOX and COX-1-derived lipids grouped together, with polyhydroxylated lipids again correlating closer with COX-1. However, this visualization also revealed a family that correlated with 16:0e/22:5(O)-PE (red arrows) (Fig. 7B). Notably, almost all were acyl-PEs and PCs, with exclusively either 22:5 or 22:4 monoxygenated fatty acids at *Sn2,* and several are p12-LOX derived. This suggests that 12-LOX forms 22:4(O) or 22:5(O) PLs that regulated as a group. Along with the heatmap, this further supports the idea of differential behavior, based on the *Sn2* oxidized fatty acid composition. For both heatmap and correlation analyses, we normalized all lipids to the mean of the control unstimluated values. In that way, we examined how each lipid behaves individually, relating to activation or health/disease. There are major differences in abundance between individual lipids, e.g. HETE-containing PLs predominate while lipids from less abundant fatty acids, or with multiple oxygens are present in lower amounts (13). If data is not normalized, then correlations will be influenced by amounts rather than biological pathways. We also generated correlations where we separated out APS and HC datasets. While these appear visually distinct, the same trends where 12-LOX derived lipids or COX-1/polyoxygenated lipids correlated in groups due to biological pathway was maintained (fig S4).

We then characterized the 47 lipids using a network analysis (Cytoscape 3.2.1), where nodes represent individual lipids and degree (size) is determined by the number of links to others (Fig. 8A). Edge thickness represents the strength of correlation between individual nodes. Nodes with the highest degree cluster toward the center. The network

diagram illustrates that COX-1 and p12-LOX derived lipids behave as two separate groups, with only a small degree of relatedness between them. The analysis further showed all remaining 20:4(3O) lipids locate with COX-1, suggesting them to be prostaglandin (PG)-containing PLs. Four PEs correlated with p12-LOX, indicating this as their origin. When analyzed as a single group, the thirty one p12-LOX derived eoxPL were significantly elevated in APS platelets both basally and following thrombin stimulation, while for COX-1 derived eoxPL, a trend towards higher amounts in APS was noted (Fig. 8B). Last, a group of exclusively plasmalogen mono or dioxygenated-PEs from 22:5 or 20:4 behaved as a separate family, suggesting a different enzymatic origin to either COX-1 or p12-LOX (Fig. 8 A). Unlike COX-1 and p12-LOX derived eoxPL, these lipids did not elevate on thrombin activation and were present basally (fig. S3). It is also noteworthy that COX-1 eoxPL in this group are exclusively plasmalogen species, while p12-LOX-derived include both acyl and plasmalogen forms as well as PC and PE.

Discussion

Herein, we show using in vitro coagulation studies, murine venous thrombosis models and molecular dynamics simulations that HETE-PLs increase calcium/PS-dependent factor activities in vitro and in vivo (Figs. 1 to 4). Coagulation factors associate with anionic phospholipids (classically native PS and PE) via interactions with positively charged calcium ions. Positioning the HETE hydroxyl group near the membrane surface appears to enhance this, and provides a mechanistic basis (Fig. 2). Mice lacking either 12/15-LOX (leukocyte type) or p12-LOX (platelet type) were affected in venous bleeding challenge models, indicating that both LOX isoforms likely act in

concert to achieve effective hemostasis in vivo (Fig. 4). Circulating blood cells from patients with the thrombotic disorder APS had significantly higher amounts of leukocyte and platelet-derived eoxPL basally, in concert with elevated anti-HETE-PL immunoreactivity (Figs. 5 to 6). Furthermore, by undertaking a comprehensive lipidomics analysis of platelets from APS patients and controls, a complex network of independently-regulated eoxPL families from COX-1 and p12-LOX was revealed (Figs. 7 to 8). A large group of platelet lipids, generated via p12-LOX, were significantly elevated in APS (Fig. 8B). Together, this suggests a contribution of eoxPL from this pathway to human thrombotic disease via their procoagulant or immunogenic activities, but this remains to be conclusively proven. The clear stratification of lipids into groups that behaved differently based on headgroup, *Sn2* fatty acid or *Sn1* acyl/plasmalogen composition shown by the clustering/network analyses suggests additional enzymatic regulation mechanisms for eoxPL formation and metabolism in platelets, that remain to be characterized. These could include differential enzymatic control of acylation of the oxidized fatty acids into specific lysoPL species. In this regard, little is yet known about fatty acyl CoA ligase or lysophospholipid acyl-transferase isoform preference for different oxidized fatty acids or eicosanoids as substrates for esterification, in platelets or any cell type.

Previous studies proposed a role for lipid oxidation in APS since non-enzymatic oxidation products increase in urine (28). We suggest that this may be initiated by leukocyte and platelet LOXs, with primary enzymatic oxidation products such as peroxides and lipid radicals decomposing and mediating propagation reactions non-enzymatically. While there are numerous antigenic targets for antiphospholipid antibodies, only some have been implicated in APS (29,30). Further study is necessary to determine whether HETE-PE-specific antibodies are causally involved, however

elevated IgG indicates that the lipids will be chronically elevated in APS patients with thrombotic disease.

A mechanism proposed to promote thrombosis in APS involves increased binding of β2GPI to PF4, causing platelet activation measured by elevated in vivo TXB_2 (31-33). In this regard, we found HETE-PEs facilitated increased β2GPI binding to membranes, both directly and *via* enhancing cardiolipin-dependent binding, and also observed elevated TXB_2 in vivo in our cohort (Fig. 5E, 6, D and E). Additionally, APS monocytes can promote both coagulation and inflammation via elevated tissue factor (TF), TNFa and IL-1 generation (34,35). It is known that β2GPI binding to monocytes in complex with anti-β2GPI IgG increases TF (36). Thus, our studies suggest two potential mechanisms for elevated thrombosis linked to eoxPL: (i) direct HETE-PL enhancement of PS-dependent coagulation on the platelet or leukocyte surface, by mechanisms characterized herein, and (ii) increased β2GPI binding to oxidized phospholipids on the surface of circulating immune cells, which then goes on to promote inflammation and TF expression. Further work is required to determine the relative contribution of these to APS. We also noted a significant elevation in the neutrophil 5-LOX-derived 5-HETE-PE and 5-HETE-PE IgG indicating that these cells circulate in an activated state in APS (Figs. 5B, 6B) (37). Since 5-HETE-PE also increased cardiolipin-dependent b2GPI membrane binding, potentially mimicking apoptosis, this could enhance neutrophil activation and clearance already known to occur in APS (Fig. 6E) (38).

Coagulation factors FII, VII, IX and X contain Gla domains, specialized regions that contain post-translational modifications of many glutamate residues by vitamin K-dependent carboxylation to form γ-carboxyglutamate. These mediate a high-affinity interaction of calcium with aPL on the cell surface, in particular PS and PE (2,23). The cofactors FVIII and FV bind negatively charged phospholipids via the homologous C1

and C2 domains. HETE-PLs enhanced coagulation in vitro and in vivo (Figs. 1,3,4). It is well known that native PC alone does not support coagulation, since its bulky head group inhibits Gla domain interactions with its phosphate (2). However, in multiple experiments in vitro and in vivo, HETE-PC promoted coagulation (Fig. 1, D to F, 3A). Most previous studies have focused on the head group, however PLs also differ with respect to fatty acid composition (3,26). Thus, the action of eoxPL is entirely dependent on the oxidized epitope. This represents a paradigm shift in our understanding of hemostasis, whereby certain forms of PC rapidly generated by activated leukocytes and platelets promote clotting. Dissecting out which specific factors and co-factors are sensitive to HETE-PLs will be undertaken using recombinant factors and surface plasmon resonance in a follow-on study.

HETE-PLs directly enhanced PS-dependent thrombin generation, suggesting they act similarly to native PE *via* calcium binding (Fig. 1, G to J). Our molecular dynamics simulation strongly supports this (Fig. 2). The HETE-hydroxyl group quickly moved ~~on~~ to the surface of the membrane, where it is able to interact with calcium. It also widened the distance between headgroups allowing greater accessibility to phosphate. To some extent, the effect of HETE-PL mimics the role of the carboxylic acid of the PS headgroup, which offers an anchor to calcium, and this was backed by showing increased calcium association with HETE-PE liposomes (Fig. 2F).

This process also provides a potential explanation for elevated β2GP1 binding. Cardiolipin is negatively-charged at pH 7.4. Although it contains two phosphate groups, the pKa values are such that one is protonated and one is not at pH 7.4, giving an overall net negative charge. In a similar way to PS, we hypothesise through pushing upwards, the HETE group may allow cardiolipin phosphates to interact more effectively with the positively-charged β2GP1.

Concentrations of HETE-PLs in thrombinoscope assays ranged from 10 - 100 ng/ml. We calculated HETE-PL generation by human or mouse platelets to be 23 ng/4 x 10^7, or 35 ng/2 x 10^8 for human or murine platelets respectively (9) (Fig. 3D). Given typical blood platelet concentrations (2 or 4 x 10^8/ml for human or mouse respectively) this would be expected to equate to around 120 ng/ml or 70 ng/ml for mouse or human blood. HETE-PE and -PC isomers represent only a small fraction of the total membrane oxidation that occurs during platelet activation, with more than 100 individual molecular species being formed acutely (13). Thus the actual concentration of potential pro-coagulant eoxPLs in the platelet membrane is likely to be considerably higher than our estimates. Furthermore, recent studies showed that annexin V binding is clustered to discrete domains of the activated platelet membrane, where procoagulant PLs concentrate, thus achieving even higher local amounts (39).

p12-LOX$^{-/-}$ mice ~~show~~ have increased venous tail bleeding (40,41). We show herein that hemostasis is restored in both p12- and 12/15-LOX$^{-/-}$ mice through administering liposomes that promote clotting factor activities in vitro and elevate TATs in vivo. Since liposomes themselves do not aggregate, this indicates they act solely through providing a pro-coagulant surface. These data support the idea that coagulation is defective in these mice rather than platelet aggregation (Fig. 4 C,D). The earliest study on p12-LOX$^{-/-}$ mice reported normal platelet aggregation to most agonists, with a slight hyper-responsiveness to ADP, indicating no functional deficit (42). Venous thrombosis as studied herein, is predominantly dependent on coagulation, rather than platelet function. In this regard, APS venous thrombosis responds best to anticoagulation (e.g. warfarin, heparin) but less well to antiplatelet therapies (aspirin, clopidogrel). While our data suggest that eoxPL contribute to the thrombotic phenotype in APS in the absence of

orally active LOX inhibitors, and with the patients on oral anticoagulant therapy, it is not currently possible to test this conclusively.

We used oxPL generated by chemical/air oxidation that were purified using HPLC, since it is not currently possible to use enzymes to generate sufficient amounts for biological studies (except for 15-HETE-PE). Regardless of how the lipids are generated, they will be virtually identical, with the only difference being enantiomeric composition. Specifically, mammalian immune cell LOXs generate the S enantiomer, while air/chemical oxidation will result in an approximate 50:50 mixture of S and R enantiomers. In the case of our biological studies, where pro-coagulant activity is not based on a receptor dependent effect and is instead related to electronegative character, we do not expect S or R enantiomers to differ. Indeed, our observation that several positional isomers and both PE and PC forms were pro-coagulant supports this idea.

In summary, we demonstrate families of eoxPL elevated during APS that provide an immunogenic target, a binding site for β2GPI, and can promote coagulation in vitro and in vivo. We also characterize the mechanism by which they enhance coagulation, and show their ability to support normal hemostasis in mice. Using lipidomics and correlation networks we uncover enzymatic control pathways for multiple families of eoxPLs generated by activated platelets. The findings define mechanisms by which physiological membrane oxidation regulates innate immune cell function during acute activation/inflammation, as well as potentially leading to new diagnostic tools or treatments for bleeding or thrombotic disease.

Materials and Methods

Materials. HETE-PEs and –PCs were generated and purified as previously described (43). All other reagents are listed in Supplementary Methods.

Study Design. All studies were carried out in accordance with the principles of the Declaration of Helsinki and with informed consent and full ethical approval, as detailed in Methods. Antiphospholipid syndrome: The study was approved by the South West Wales Research Ethics Committee (12/WA/0229). Full information on patients and inclusion/exclusion criteria is in Supplementary Data1. Blood donations from healthy volunteers were approved by the Cardiff University School of Medicine Ethics Committee, and were with informed consent (SMREC 12/37, SMREC 12/10). A power calculation was not undertaken as preliminary data was not available for our studies. Rules for stopping data collection were not defined. Outliers were not removed and endpoints were not prospectively selected. Replicates for all experiments are included in figure legends. The objectives of the research were to define whether eoxPL were able to modulate coagulation reactions, determine mechanisms involved and examine whether they are elevated in human thrombotic disease. Research subjects included patients with APS (total number 18) and healthy controls (total number 34), mice (wild type and genetically modified) and liposomes of defined composition. There were several different studies in our design, including controlled laboratory experiments and observational studies. Treatments, types of observations and measurement techniques are all outlined below and in Supplementary Methods. Randomization is not relevant as we did not

conduct a clinical trial. Blinding was used during analysis of lipids from patients and controls, but not in animal, cellular or liposome experiments.

Generation of liposomes. Liposomes were made by freeze thaw, followed by extrusion in 20 mmol/L HEPES, 100 mmol/L NaCl, pH 7.35 (buffer A). Where HETE-PE was substituted for unoxidized PE, the liposomes were: 5 % SAPS, 20-30 % SAPE, 0-10 % HETE-PE and 65 % DSPC (mol %). Where unoxidized PC was substituted for HETE-PC the liposomes were: 5 % SAPS, 30 % SAPE, 55 % DSPC, 0-10 % SAPC and 0-10 % HETE-PC. Liposomes were made in the presence of 10 pmol/L full length recombinant TF, and used at a final concentration of 4 μM total lipid unless otherwise stated. Binding of β2GP1 to liposomes was determined as described in Supplementary Methods.

Thrombin generation assays. Thrombin generation assays were performed using a Fluoroskan Ascent plate reader (ThermoLabsystems, Helsinki, Finland). Cleavage of prothrombin to thrombin was measured using 0.5 mmol/L fluorogenic substrate Z-Gly-Gly-Arg-AMC and thrombin activity compared to thrombin calibrator (Stago). Thrombin generation was calculated from raw fluorescence data (44). Cleavage of prothrombin to thrombin in simplified coagulation cascade experiments was performed according to the same methods but using a mixture of FII (1.4 μmol/L), FV (26 nmol/L), FVII (10 nmol/L), FVIII (300 pmol/L), FIX (80 nmol/L) and FX (136 nmol/L) was used in buffer A with 1 % BSA (buffer B). The reaction was initiated by addition of $CaCl_2$ (20 mmol/L) and fluorogenic substrate (0.5 mmol/L) in buffer B.

Lipid extraction and analysis. 1,2-dimyristoyl-PE or -PC (10 ng) was added to each sample before extraction as an internal standard. Lipids were extracted by adding a solvent mixture (1 M acetic acid, 2-propanol, hexane (2:20:30)) to the sample at a ratio of 2.5 ml solvent mixture to 1 ml sample, vortexing and then adding 2.5 ml of hexane. Following vortexing and centrifugation (400 g, 5 mins), lipids were recovered in the upper hexane layer. The samples were then re-extracted by the addition of an equal volume of hexane followed by further vortexing and centrifugation. The combined hexane layers were then dried under vacuum and analyzed for HETE-PE using LC/MS/MS. Samples were separated on a C_{18} Luna, 3 µm, 150 mm x 2mm column (Phenomenex) gradient of 50-100 % B over 10 min followed by 30 min at 100 % B (Solvent A: methanol:acetonitrile:water, 1 mM ammonium acetate, 60:20:20. Solvent B: methanol, 1 mM ammonium acetate) with a flow rate of 200 µl/min. Electrospray mass spectra were obtained on a Q-Trap instrument (Applied Biosystems 4000 Q-Trap) operating in the negative mode. Products were analyzed in the MRM mode monitoring transitions from the parent ion to daughter ion of 179.1 (12 HETE $[M-H]^-$) every 200 ms with a collision energy of -45-42V. The area under the curve for the parent to 179.1 was integrated and normalized to the internal standard for 16:0p, 18:1p/ 18:0p and 18:0a/12-HETE-PEs. For quantification of these lipids, standard curves were generated with purified 18:0a/12-HETE-PE/PC. Where large numbers of HETE-PLs were measured in lipidomics assays, fold changes relative to PE or PC internal standards were determined using MRM transitions recently published (13).

Determination of circulating antibodies to HETE-PEs. Specific Ab titres to individual HETE-PEs were determined by chemiluminescent ELISA as previously described, with further details in Supplementary Methods (45).

Isolation of human washed platelets. Washed platelets were prepared from whole blood drawn from a central venous catheter into syringes containing acidified citrate dextrose (ACD; 85 mM trisodium citrate, 65 mM citric acid, 100 mM glucose) at a ratio of 8.1 parts whole blood to 1.9 parts ACD, as described previously (46), and resuspended in modified Tyrode's buffer (134 mM NaCl, 12 mM $NaHCO_3$, 2.9 mM KCl, 0.34 mM Na_2HPO_4, 1.0 mM $MgCl_2$, 10mM HEPES, 5mM glucose, pH 7.4) at 2 x 10^8/mL. 1 ml platelets was incubated at 37 ^oC for 30 min with 1 mM $CaCl_2$, 0.2 U/mL human thrombin (Sigma-Aldrich, UK) or modified Tyrode's buffer.

Isolation and activation of human leukocytes, and murine platelets. Leukocytes were prepared from whole blood drawn from a venous catheter with full details in Supplementary Methods. Leukocytes were isolated from 20 ml citrate anticoagulated whole blood. Leukocytes were activated at 37 °C with 10 μM A23187 in the presence of 1 mmol/$CaCl_2$, for 30 min. Mouse platelets were isolated as described in Supplementary Methods, then activated with 0.2 U/ml thrombin and 1 mM $CaCl_2$ followed by gentle mixing every 2 - 3 min for 30 min at 37 °C.

Isolation of serum, plasma and urine. Full details are provided in Supplementary Methods. 11-dehyro-TxB_2 was measured using GC/MS as previously described (47). Plasma thrombin-antithrombin complexes were determined using a commercial ELISA as in Supplementary Methods.

Quantification of blood loss from tail bleeding assays. C57/BL6 wild type (Charles River), 12/15-LOX$^{-/-}$ and p12-LOX$^{-/-}$ mice bred in-house were kept in constant temperature cages (20 – 22 °C) and given free access to water and standard chow. Tail bleeding assays and breeding of mice was performed under Home Office License PPL/3150. Full details on procedure, liposome composition and blood loss measurements are given in Supplementary Methods.

Injury-related venous thrombosis. Thrombosis was induced as described previously with minor modifications (48), as described in Supplementary Methods.

Lipid Bilayer Model Preparation, and membrane energy minimization and simulation protocol. A pre-equilibrated hydrate lipid bilayer consisting of 128 molecules of 1,2-Dioleoyl-sn-glycero-3-phosphocholine (DOPC), based on a previously reported study, was downloaded from the ATM database (Box ID: 30) (49,50). Full details of the protocol are provided in Supplementary Methods.

Measurement of calcium binding to membranes. Binding of calcium to lipids was determined by competition with a calcium probe, Fluo-FF, as described in Supplementary Methods.

Heatmap and Cytoscape correlation. Heatmaps were generated using the pheatmap package in R (version 3.3.1). Data was first normalised to the mean of the unstimulated control values for each lipid. Network analysis was performed with Cytoscape (version 3.4.0), utilizing pairwise correlations between lipids generated with R. The network

diagram shows only correlations with a Pearson product-moment correlation coefficient value (r) > 0.8, due to the high number of interactions.

Statistics

Statistical significance was calculated using Mann Whitney U test, unless otherwise stated. The statistical differences between β2GPI binding to HETE-PL and cardiolipin liposomes were calculated using one-way ANOVA with Tukey-Kramers multi comparison post hoc test, used to compare the means of each condition. p values of < 0.05 were considered significant (*), values of $p < 0.01$ considered highly significant (**), with values of $p < 0.001$ considered exceptionally significant (***). Statistical analysis was performed using Graphpad Prism 6. Unless otherwise stated in figure legends, data displayed as tukey boxplots, where whiskers represent 1.5 the lower and upper interquartile range, data not included within the whiskers is displayed as individual outliers. The correlation plot (Fig. 7B) was created in R using the corrplot package (51,52).

List of Supplementary Materials:

Supplementary Data.docx (full description of methods that could not be included due to word limits and supplementary figs S1 to S4: bar charts for all lipids measured in APS or 12-LOX-/- study, additional correlation plots, analysis of patient demographics)

lipid simulation.avi (movie showing 300 ns simulation of 12-HETE-PC in a membrane)

statsletter.doc (email from Dr Farewell confirming stats).

References

1. Falls, L. A., Furie, B., and Furie, B. C. Role of phosphatidylethanolamine in assembly and function of the factor IXa-factor VIIIa complex on membrane surfaces. *Biochemistry* **39**, 13216-13222 (2000)
2. Tavoosi, N., Davis-Harrison, R. L., Pogorelov, T. V., Ohkubo, Y. Z., Arcario, M. J., Clay, M. C., Rienstra, C. M., Tajkhorshid, E., and Morrissey, J. H. Molecular determinants of phospholipid synergy in blood clotting. *The Journal of biological chemistry* **286**, 23247-23253 (2011)
3. Clark, S. R., Thomas, C. P., Hammond, V. J., Aldrovandi, M., Wilkinson, G. W., Hart, K. W., Murphy, R. C., Collins, P. W., and O'Donnell, V. B. Characterization of platelet aminophospholipid externalization reveals fatty acids as molecular determinants that regulate coagulation. *Proceedings of the National Academy of Sciences of the United States of America* **110**, 5875-5880 (2013)
4. Clark, S. R., Guy, C. J., Scurr, M. J., Taylor, P. R., Kift-Morgan, A. P., Hammond, V. J., Thomas, C. P., Coles, B., Roberts, G. W., Eberl, M., Jones, S. A., Topley, N., Kotecha, S., and O'Donnell, V. B. Esterified eicosanoids are acutely generated by 5-lipoxygenase in primary human neutrophils and in human and murine infection. *Blood* **117**, 2033-2043 (2011)
5. Hammond, V. J., Morgan, A. H., Lauder, S., Thomas, C. P., Brown, S., Freeman, B. A., Lloyd, C. M., Davies, J., Bush, A., Levonen, A. L., Kansanen, E., Villacorta, L., Chen, Y. E., Porter, N., Garcia-Diaz, Y. M., Schopfer, F. J., and O'Donnell, V. B. Novel keto-phospholipids are generated by monocytes and macrophages, detected in cystic fibrosis, and activate peroxisome proliferator-activated receptor-gamma. *The Journal of biological chemistry* **287**, 41651-41666 (2012)

6. Maskrey, B. H., Bermudez-Fajardo, A., Morgan, A. H., Stewart-Jones, E., Dioszeghy, V., Taylor, G. W., Baker, P. R., Coles, B., Coffey, M. J., Kuhn, H., and O'Donnell, V. B. Activated platelets and monocytes generate four hydroxyphosphatidylethanolamines via lipoxygenase. *The Journal of biological chemistry* **282**, 20151-20163 (2007)
7. Morgan, A. H., Dioszeghy, V., Maskrey, B. H., Thomas, C. P., Clark, S. R., Mathie, S. A., Lloyd, C. M., Kuhn, H., Topley, N., Coles, B. C., Taylor, P. R., Jones, S. A., and O'Donnell, V. B. Phosphatidylethanolamine-esterified eicosanoids in the mouse: tissue localization and inflammation-dependent formation in Th-2 disease. *The Journal of biological chemistry* **284**, 21185-21191 (2009)
8. Morgan, L. T., Thomas, C. P., Kuhn, H., and O'Donnell, V. B. Thrombin-activated human platelets acutely generate oxidized docosahexaenoic-acid-containing phospholipids via 12-lipoxygenase. *Biochem J* **431**, 141-148 (2010)
9. Thomas, C. P., Morgan, L. T., Maskrey, B. H., Murphy, R. C., Kuhn, H., Hazen, S. L., Goodall, A. H., Hamali, H. A., Collins, P. W., and O'Donnell, V. B. Phospholipid-esterified eicosanoids are generated in agonist-activated human platelets and enhance tissue factor-dependent thrombin generation. *The Journal of biological chemistry* **285**, 6891-6903 (2010)
10. O'Donnell, V. B., and Murphy, R. C. New families of bioactive oxidized phospholipids generated by immune cells: identification and signaling actions. *Blood* **120**, 1985-1992 (2012)
11. Aldrovandi, M., Hammond, V. J., Podmore, H., Hornshaw, M., Clark, S. R., Marnett, L. J., Slatter, D. A., Murphy, R. C., Collins, P. W., and O'Donnell, V. B. Human platelets generate phospholipid-esterified prostaglandins via

cyclooxygenase-1 that are inhibited by low dose aspirin supplementation. *Journal of lipid research* **54**, 3085-3097 (2013)

12. Aldrovandi, M., Hinz, C., Lauder, S. N., Podmore, H., Hornshaw, M., Slatter, D. A., Tyrrell, V. J., Clark, S. R., Marnett, L. J., Collins, P. W., Murphy, R. C., and O'Donnell, V. B. DioxolaneA3-phosphatidylethanolamines are generated by human platelets and stimulate neutrophil integrin expression. *Redox biology* **11**, 663-672 (2017)
13. Slatter, D. A., Aldrovandi, M., O'Connor, A., Allen, S. M., Brasher, C. J., Murphy, R. C., Mecklemann, S., Ravi, S., Darley-Usmar, V., and O'Donnell, V. B. Mapping the Human Platelet Lipidome Reveals Cytosolic Phospholipase A2 as a Regulator of Mitochondrial Bioenergetics during Activation. *Cell metabolism* **23**, 930-944 (2016)
14. Keeling, D., Mackie, I., Moore, G. W., Greer, I. A., Greaves, M., and British Committee for Standards in, H. Guidelines on the investigation and management of antiphospholipid syndrome. *British journal of haematology* **157**, 47-58 (2012)
15. de Groot, P. G., and Urbanus, R. T. The significance of autoantibodies against beta2-glycoprotein I. *Blood* **120**, 266-274 (2012)
16. McNally, T., Mackie, I. J., Machin, S. J., and Isenberg, D. A. Elevated levels of beta 2 glycoprotein-I (beta 2 GPI) in antiphospholipid antibody syndrome are due to increased amounts of beta 2 GPI in association with other plasma constituents. *Blood Coagul Fibrinolysis* **6**, 411-416 (1995)
17. Morrissey, J. H., Tajkhorshid, E., and Rienstra, C. M. Nanoscale studies of protein-membrane interactions in blood clotting. *Journal of thrombosis and haemostasis : JTH* **9 Suppl 1**, 162-167 (2011)

18. Zwaal, R. F., and Schroit, A. J. Pathophysiologic implications of membrane phospholipid asymmetry in blood cells. *Blood* **89**, 1121-1132 (1997)

19. Mann, K. G. Biochemistry and physiology of blood coagulation. *Thrombosis and haemostasis* **82**, 165-174 (1999)

20. Lhermusier, T., Chap, H., and Payrastre, B. Platelet membrane phospholipid asymmetry: from the characterization of a scramblase activity to the identification of an essential protein mutated in Scott syndrome. *Journal of thrombosis and haemostasis : JTH* **9**, 1883-1891 (2011)

21. Schick, P. K., Kurica, K. B., and Chacko, G. K. Location of phosphatidylethanolamine and phosphatidylserine in the human platelet plasma membrane. *The Journal of clinical investigation* **57**, 1221-1226 (1976)

22. Majumder, R., Liang, X., Quinn-Allen, M. A., Kane, W. H., and Lentz, B. R. Modulation of prothrombinase assembly and activity by phosphatidylethanolamine. *The Journal of biological chemistry* **286**, 35535-35542 (2011)

23. Huang, M., Rigby, A. C., Morelli, X., Grant, M. A., Huang, G., Furie, B., Seaton, B., and Furie, B. C. Structural basis of membrane binding by Gla domains of vitamin K-dependent proteins. *Nature structural biology* **10**, 751-756 (2003)

24. Lu, J., Pipe, S. W., Miao, H., Jacquemin, M., and Gilbert, G. E. A membrane-interactive surface on the factor VIII C1 domain cooperates with the C2 domain for cofactor function. *Blood* **117**, 3181-3189 (2011)

25. Ngo, J. C., Huang, M., Roth, D. A., Furie, B. C., and Furie, B. Crystal structure of human factor VIII: implications for the formation of the factor IXa-factor VIIIa complex. *Structure* **16**, 597-606 (2008)

26. Zwaal, R. F., Comfurius, P., and Bevers, E. M. Lipid-protein interactions in blood coagulation. *Biochimica et biophysica acta* **1376**, 433-453 (1998)

27. Chaturvedi, S., Alluri, R., and McCrae, K. R. Extracellular Vesicles in the Antiphospholipid Syndrome. *Semin Thromb Hemost* (2017)

28. Pratico, D., Ferro, D., Iuliano, L., Rokach, J., Conti, F., Valesini, G., FitzGerald, G. A., and Violi, F. Ongoing prothrombotic state in patients with antiphospholipid antibodies: a role for increased lipid peroxidation. *Blood* **93**, 3401-3407 (1999)

29. Lim, W., and Crowther, M. A. Antiphospholipid antibiodies: a critical review of the literature. *Curr Opin Hematol* **14**, 494-499 (2007)

30. Misasi, R., Capozzi, A., Longo, A., Recalchi, S., Lococo, E., Alessandri, C., Conti, F., Valesini, G., and Sorice, M. "New" antigenic targets and methodological approaches for refining laboratory diagnosis of antiphospholipid syndrome. *J Immunol Res* **2015**, 858542 (2015)

31. Vega-Ostertag, M., Harris, E. N., and Pierangeli, S. S. Intracellular events in platelet activation induced by antiphospholipid antibodies in the presence of low doses of thrombin. *Arthritis Rheum* **50**, 2911-2919 (2004)

32. Sikara, M. P., Routsias, J. G., Samiotaki, M., Panayotou, G., Moutsopoulos, H. M., and Vlachoyiannopoulos, P. G. {beta}2 Glycoprotein I ({beta}2GPI) binds platelet factor 4 (PF4): implications for the pathogenesis of antiphospholipid syndrome. *Blood* **115**, 713-723 (2010)

33. Lutters, B. C., Derksen, R. H., Tekelenburg, W. L., Lenting, P. J., Arnout, J., and de Groot, P. G. Dimers of beta 2-glycoprotein I increase platelet deposition to collagen via interaction with phospholipids and the apolipoprotein E receptor 2'. *The Journal of biological chemistry* **278**, 33831-33838 (2003)

34. Xie, H., Zhou, H., Wang, H., Chen, D., Xia, L., Wang, T., and Yan, J. Anti-beta(2)GPI/beta(2)GPI induced TF and TNF-alpha expression in monocytes

involving both TLR4/MyD88 and TLR4/TRIF signaling pathways. *Mol Immunol* **53**, 246-254 (2013)

35. Lopez-Pedrera, C., Buendia, P., Cuadrado, M. J., Siendones, E., Aguirre, M. A., Barbarroja, N., Montiel-Duarte, C., Torres, A., Khamashta, M., and Velasco, F. Antiphospholipid antibodies from patients with the antiphospholipid syndrome induce monocyte tissue factor expression through the simultaneous activation of NF-kappaB/Rel proteins via the p38 mitogen-activated protein kinase pathway, and of the MEK-1/ERK pathway. *Arthritis Rheum* **54**, 301-311 (2006)

36. Sorice, M., Longo, A., Capozzi, A., Garofalo, T., Misasi, R., Alessandri, C., Conti, F., Buttari, B., Rigano, R., Ortona, E., and Valesini, G. Anti-beta2-glycoprotein I antibodies induce monocyte release of tumor necrosis factor alpha and tissue factor by signal transduction pathways involving lipid rafts. *Arthritis Rheum* **56**, 2687-2697 (2007)

37. Arvieux, J., Jacob, M. C., Roussel, B., Bensa, J. C., and Colomb, M. G. Neutrophil activation by anti-beta 2 glycoprotein I monoclonal antibodies via Fc gamma receptor II. *J Leukoc Biol* **57**, 387-394 (1995)

38. Levine, J. S., Subang, R., Koh, J. S., and Rauch, J. Induction of anti-phospholipid autoantibodies by beta2-glycoprotein I bound to apoptotic thymocytes. *J Autoimmun* **11**, 413-424 (1998)

39. Whyte, C. S., Swieringa, F., Mastenbroek, T. G., Lionikiene, A. S., Lance, M. D., van der Meijden, P. E., Heemskerk, J. W., and Mutch, N. J. Plasminogen associates with phosphatidylserine-exposing platelets and contributes to thrombus lysis under flow. *Blood* **125**, 2568-2578 (2015)

40. Yeung, J., Apopa, P. L., Vesci, J., Stolla, M., Rai, G., Simeonov, A., Jadhav, A., Fernandez-Perez, P., Maloney, D. J., Boutaud, O., Holman, T. R., and Holinstat,

M. 12-lipoxygenase activity plays an important role in PAR4 and GPVI-mediated platelet reactivity. *Thrombosis and haemostasis* **110**, 569-581 (2013)

41. Yeung, J., Tourdot, B. E., Fernandez-Perez, P., Vesci, J., Ren, J., Smyrniotis, C. J., Luci, D. K., Jadhav, A., Simeonov, A., Maloney, D. J., Holman, T. R., McKenzie, S. E., and Holinstat, M. Platelet 12-LOX is essential for FcgammaRIIa-mediated platelet activation. *Blood* **124**, 2271-2279 (2014)
42. Johnson, E. N., Brass, L. F., and Funk, C. D. Increased platelet sensitivity to ADP in mice lacking platelet-type 12-lipoxygenase. *Proceedings of the National Academy of Sciences of the United States of America* **95**, 3100-3105 (1998)
43. Morgan, A. H., Hammond, V. J., Morgan, L., Thomas, C. P., Tallman, K. A., Garcia-Diaz, Y. R., McGuigan, C., Serpi, M., Porter, N. A., Murphy, R. C., and O'Donnell, V. B. Quantitative assays for esterified oxylipins generated by immune cells. *Nat Protoc* **5**, 1919-1931 (2010)
44. Hemker, H. C., Giesen, P. L., Ramjee, M., Wagenvoord, R., and Beguin, S. The thrombogram: monitoring thrombin generation in platelet-rich plasma. *Thrombosis and haemostasis* **83**, 589-591 (2000)
45. Horkko, S., Miller, E., Dudl, E., Reaven, P., Curtiss, L. K., Zvaifler, N. J., Terkeltaub, R., Pierangeli, S. S., Branch, D. W., Palinski, W., and Witztum, J. L. Antiphospholipid antibodies are directed against epitopes of oxidized phospholipids. Recognition of cardiolipin by monoclonal antibodies to epitopes of oxidized low density lipoprotein. *The Journal of clinical investigation* **98**, 815-825 (1996)
46. Thomas, C. P., Clark, S. R., Hammond, V. J., Aldrovandi, M., Collins, P. W., and O'Donnell, V. B. Identification and quantification of aminophospholipid molecular species on the surface of apoptotic and activated cells. *Nat Protoc* **9**, 51-63 (2014)

47. Morrow, J. D., and Minton, T. A. Improved assay for the quantification of 11-dehydrothromboxane B2 by gas chromatography-mass spectrometry. *J Chromatogr* **612**, 179-185 (1993)

48. Wang, X., and Xu, L. An optimized murine model of ferric chloride-induced arterial thrombosis for thrombosis research. *Thromb Res* **115**, 95-100 (2005)

49. *Automated Topology Builder (ATB) and Repository. Version 2.2. Accessed on 1/7/2015*

50. Poger, D., Mark, A.E. On the Validation of Molecular Dynamics Simulations of Saturated and cis-Monounsaturated Phosphatidylcholine Lipid Bilayers: A Comparison with Experiment *J. Chem. Theory Comput* **6**, 11 (2010)

51. R Core Team (2016) R: A language and environment for statistical computing. in *R Foundation for Statistical Computing, Vienna, Austria. URL*, https://www.R-project.org/.

52. Wei, T., Simko, V. (2016) corrplot: Visualization of a Correlation Matrix. R package version 0.77. in , https://CRAN.R-project.org/package=corrplot

53. Coates, R., Firsan SJ. Thioimidate N-oxides: nitrones of thio esters. *J Org Chem* **51**, 12 (1986)

54. *Molecular Operating environment, version 2014.09. Chemical Computing Group, Montreal, Canada*

55. *Schrödinger Release 2014-1: Desmond Molecular Dynamics System, version 3.7, D. E. Shaw Research, New York, NY, 2014. Maestro-Desmond Interoperability Tools, version 3.7, Schrödinger, New York, NY, 2014*,

56. Bowers, K., Chow, E, Xu, H, Dror, RO, Eastwood, MP, Gregersen, BA, Klepeis, JL, Kolossvary, I, Moraes, MA, Sacerdoti, FD, Salmon, JK, Shan, Y, Shaw, DE. (2006) Scalable Algorithms for Molecular Dynamics Simulations on Commodity

Clusters. in *Proceedings of the ACM/IEEE Conference on Supercomputing (SC06), Tampa, Florida,*

Acknowledgements:

We thank patients and volunteers for taking part in these studies. Funding is acknowledged from Wellcome Trust (094143/Z/10/Z), European Research Council (LipidArrays, VBO) and British Heart Foundation (RG/12/11/29815) (VBO, PWC), British Heart Foundation Research Fellowship (FS/11/42/28753) (CLP), the Else-Kröner Fresenius Stiftung (to GK) and The Life Sciences Research Network Wales (Welsh Computer-Aided Drug Design Platform). We gratefully acknowledge assistance with tail bleeding from Dr Christopher Williams, for Nanosight experiments from Mark Gurney, for patient recruitment from Mrs Claire Nott, and technical support from Dr Christopher Rice

Author Contributions.

Experiments were conducted by SNL, DAS, GM, RU, AOC, DF, JM, SR, VJT, AB, SF, MA, MH, KAR, CPT, JA and GK, and designed by SNL, DAS, PDG, SH, VBO, SAJ, PRT, PWC, PVJ. CLP and SO provided clinical samples. AP provided supervision and training. SNL, DAS, VBO and PWC wrote the paper. All authors edited the manuscript.

Conflict of Interest Disclosures

The authors have declared that no conflict of interest exist

Figure Legends

Figure 1. HETE-PE/PCs dose dependently enhance TF-dependent thrombin generation through a PS-dependent mechanism. Thrombin generation was initiated by addition of liposomes to pooled platelet poor plasma (PPP) as described in Methods, using a thrombinoscope. *Panels A-C. HETE-PEs enhance TF-dependent coagulation in*

plasma. Liposomes contained 10 pM recombinant TF with 65 % DSPC, 5 % SAPS and 30 % SAPE, with 0 – 10 % SAPE replaced with 0 – 10 % HETE-PE. *(A)* 5-HETE-PE, *(B)* 12-HETE-PE, *(C)* 15-HETE-PE. *Panels D-F. HETE-PCs enhance TF-dependent coagulation in plasma.* Liposomes contained 10 pM TF, 55 % DSPC, 5 % SAPS, 30 % SAPE, with 0 – 10 % SAPC replaced with < 10 % HETE-PC. *(D)* 5-HETE-PC, *(E)* 12-HETE-PC, *(F)* 15-HETE-PC. Representative traces are shown of experiments repeated at least 3 times. *Panels G-J. 15-HETE-PE/PC enhances PS-dependent thrombin generation.* Pooled PPP was activated using liposomes, as above, where SAPE was replaced with 15-HETE-PE/PC, with/without SAPS (replacing PC) as indicated on the figure. Representative traces (Panel G, I) and maximum thrombin at varying PS concentration (Panel H, J) are shown (n = 3 runs, mean ± SEM). *Panels K-M. HETE-PE/PCs promote activities of coagulation factors in a full reconstitution system.* Thrombin generation was initiated by addition of liposomes to purified factors II, V, VII, VIIII, IX, X at physiological concentrations, as described in Methods. Liposomes contained *(Panel K)* 65 % DSPC, 5 % SAPS, 30 % SAPE, with 10 % SAPE (control) or 10 % HETE-PE or *(Panel L)* 55 % DSPC, 5 % SAPS, 30 % SAPE, 10 % SAPC (control) or 10% HETE-PC. Panel M shows summary data showing fold-change for the maximum thrombin generation rate observed (slope of lines in K,L) for each isomer (n = 3 runs, mean ± SEM). ** $p<0.01$, * : $p<0.05$, single-factor ANOVA and post-hoc Tukey tests.

Figure 2. Molecular dynamics simulation demonstrates association of the HETE-PL hydroxyl group with the polar environment, serine and calcium ions, while HETE-PL membranes bind more calcium. *Panels A-E. Molecular dynamics shows HETE – OH group altering membrane behavior.* Molecular simulations were undertaken for 300 ns using 5% SAPS, 5% SAPC, 30% SAPE, 55% DOPC, 5% 12-HETE-PC as described

in Methods. *Panels A-D*. Side views showing hydrophobic (yellow), charged phosphate groups (cyan) and PC headgroups (grey). Note bending of HETE with association of –OH groups with membrane surface (Panels A), as well with calcium (Panel B,C) and the PS headgroup (Panel D). *Panel E.* Top view looking down on membrane showing areas of positive charge (blue), negative charge (brown), PS headgroups (pink) and HETE hydroxyl groups (red). Note that all three PS and HETE –OH groups are visible (labeled) from above. *Panel F. Binding of calcium to membranes is increased by 15-HETE-PE.* Liposomes comprising 65 % DSPC, 30 % SAPE, and 5 % SAPS, with up to 10 % SAPE replaced by 15-HETE PE were tested for calcium binding using by Fluo-FF fluorescence, as described in Methods. **p<0.01 and *p<0.05 show significance compared to no added 15-HETE PE (n = 3 separate samples, mean ± SEM).

Figure 3. HETE-PL liposomes prevent tail bleeding and elevate TAT levels *in vivo,* while platelets from mice genetically lacking p12-LOX fail to generate numerous eoxPL. *Panel A 12-HETE-PE/TF intra-dermal administration prevents tail bleeding in adult mice.* 11-week old male C57BL/6J mice were injected with liposomes containing TF with or without 12-HETE-PE or -PC, immediately proximal of a tail cut, and bleeding time and blood loss recorded as in Methods (n = 10 - 16 mice per group). ** $p \leq 0.01$, * $p \leq 0.05$. Mann Whitney U test *Panel B. 12-HETE-PE elevates thrombin-anti-thrombin (TAT) complexes in vivo.* Control or HETE-PE-containing liposomes were injected i.v. into wild type mice and plasma obtained after 1 hr. TAT levels were measured using ELISA as described in Methods (n = 6 mice per group, * $p \leq 0.05$). *Panel C. Murine washed platelets generate several eoxPL on thrombin activation, that are absent in p12-LOX-deficiency.* Murine washed platelets were activated for 30 min using 0.2 U/ml thrombin, then lipids extracted and analyzed for eoxPL as described in Methods (n = 3, mean).

Heatmap was generated as described in Methods using the pheatmap package in R. *Panel D. Time course of generation of 12-HETE-PEs and –PCs shows lipids continue to elevate up to at least 30 min post activation.* Platelets from wild-type or 12-LOX$^{-/-}$ mice (2 x 10^8/ml) were activated using 0.2 U/ml human thrombin for 0 - 30 min at 37 °C, and lipids then extracted and quantified as described in Methods. HETE-PE represents the sum of 16:0p/12-HETE-PE, 18:1p/12-HETE-PE, 18:0/12-HETE-PE, and 18:0a/HETE PE. HETE-PC represents the sum of 16:0a/12-HETE-PC and 18:0a/12-HETE-PC (mean ± SEM, n = 8 mice).

Figure 4. Mice lacking either 12/15- or p12-LOX have impaired venous coagulation in vivo, that can be restored using 12-HETE-PE liposome administration. *Panels A,B. p12-LOX deficient mice show lower thrombus formation in vivo following challenge.* Venous thrombosis was induced *in vivo* in p12-LOX$^{-/-}$ mice as described in Methods (n = 7-9 mice per group). A representative thrombus is shown. *Panel C. p12-LOX deficient mice have impaired hemostasis in vivo.* 8-11 week old male wild type C57BL/6J or p12-LOX$^{-/-}$ mice were administered a tail cut, and bleeding time and blood loss recorded as in Methods. Liposomes containing 19 ng 12-HETE-PE or control liposomes were administered in 10 ml PBS, just upstream of the cut, and immediately beforehand (n = 6 – 12 mice per group ** $p \leq 0.01$). *Panel D. 12/15-LOX deficient mice have impaired hemostasis in vivo.* As for Panel C, 8 - 11 week old male wild type C57BL/6J or 12/15-LOX$^{-/-}$ mice were administered a tail cut with/without liposomes, and bleeding time and blood loss recorded as in Methods (n = 12 – 19 mice per group, ** $p \leq 0.01$), Mann Whitney U test .

Figure 5. HETE-PEs are elevated in APS leukocytes and platelets. HETE-PEs were quantified as individual molecular species then combined. *Panels A,B. 15- and 5-HETE-PEs are elevated in leukocytes from APS patients.* Total leukocytes isolated as described, were stimulated at 4 x 10^6 cells/ml with 10 mM A23187 for 30 mins at 37 °C, then lipids analyzed for HETE-PEs as described in Methods (n = 34 (HC, Healthy controls), 17 (APS) people). *Panel C. 12-HETE-PEs are elevated in APS platelets*. Washed platelets were isolated and stimulated with 0.2 U/ml thrombin for 30 min at 37 °C as described in methods (n = 18 (HC), 12 (APS) people). *Panel D. APS platelets that spontaneously aggregated contain high levels of 12-HETE-PEs*. During the final washing step, a number of APS platelet isolates spontaneously aggregated (n = 7 patients). Lipids were extracted and analyzed for 12-HETE-PEs as in Methods. *Panel E. Urinary TXB_2 is elevated in APS*. Urine was extracted as described in Methods before GC/MS analysis as described in Methods (n = 32 (HC), 9 (APS)). *Panels F,G. Leukocyte-derived 15- and 5-HETE-PEs are elevated basally in APS platelets*. Platelets were prepared as in Panel C, then analyzed for HETE-PEs (n = 18 (HC), 12 (APS) people). *Panel H. Platelet derived 12-HETE-PEs are elevated basally in APS leukocytes*. Total leukocytes were isolated and stimulated at 4 x 10^6 cells/ml with 10 mm A23187 for 30 min at 37°C and then analyzed for 12-HETE-PEs as described in Methods (n = 34 (HC), n = 18 (APS) people), (*** $p \leq 0.001$, ** $p \leq 0.01$, * $p \leq 0.05$), Mann Whitney U test .

Figure 6. Circulating IgG against HETE-PEs are elevated in APS and b2BP1 binding to membranes is enhanced by HETE-PEs *Panels A-C. IgG against HETE-PEs are significantly elevated in APS plasma.* Levels of IgG antibodies to HETE-PEs were determined by diluting plasma 1:12 and testing binding to the indicated antigens as described in Methods. SAPE was used as unoxidized lipid comparison. All samples were

analyzed in triplicate (n = 18 (HC), n = 9 (APS) people). * p < 0.05, ** p 0.01, Mann Whitney U test *Panel D. IgG titers are comparable in healthy control and patient plasma.* Total IgG was determined in plasma from patients with APS and healthy controls (n = 34 (HC), n = 10 (APS) people). *Panel E. HETE-PEs enhance b2GPI binding to lipid membranes.* Binding of b2GPI to liposomes in the presence of cardiolipin or 15-HETE-PE, 5-HETE-PE or 12-HETE-PE alone was determined as described in Methods. *Panel F. HETE-PEs enhance cardiolipin-dependent b2GPI binding to lipids.* Binding of b2GPI to liposomes in the presence of cardiolipin with/without 15-HETE-PE, 5-HETE-PE or 12-HETE-PE was determined as in Panel E. For Panels D,E, n = 3 separate experiments, each in triplicate. mean ± SEM. Significance was determined using one-way ANOVA, Tukey-Kramers test * p < 0.05, ** p 0.01, *** P <0.001.

Figure 7. Lipidomic profiling of 47 eoxPL defines their enzymatic origin and regulatory networks. Washed platelets were isolated from healthy controls or APS patients and activated using thrombin (0.2 U/ml, 30 min) before lipid extraction and analysis using LC/MS/MS for 47 eoxPL as described in Methods (n = 16 HC, 10 APS people). *Panel A. p12-LOX and COX-1 derived lipids cluster into distinct families based on Sn2 fatty acid composition*. A heatmap showing effect of thrombin on individual lipid levels was generated using the pheatmap package in R using hierarchical clustering (complete linkage method) to group similar lipids. *Panel B. Plotting correlation between individual lipids illustrates additional relatedness between families of ions.* Correlations between lipids across the whole cohort were plotted in a grid, in order of decreasing correlation with 18:0a/12-HETE-PE, as described in Methods. Red: p12-LOX, blue: COX-1, green: polyoxygenated PL, black: unknown origin. Red arrows identify a group

of 6 lipids (almost all acyl with 22:5(O) or 22:4(O) at *Sn2*) that correlate as a group suggesting relatedness.

Figure 8. Cytoscape network confirms enzymatic origin of lipids, and identifies an additional group regulated independently of known pathways, and p12-LOX derived eoxPL are significantly elevated in APS platelets. *Panel A. A Cytoscape network correlation identifies three groups of eoxPL*. Cytoscape 1.2.3 correlation was performed (correlation > 0.8) using data shown in Figure 7A, with nodes as individual lipids and degree (size) determined by number of links to others. Edge thickness represents correlation between individual nodes. Lipids were identified as COX-1 or p12-LOX derived based on aspirin sensitivity or their absence in p12-LOX$^{-/-}$ mice, as described in Results. *Panel B. p12-LOX lipids are significantly elevated in APS, as a group either with/without thrombin activation.* Platelet lipids identified as originating from p12-LOX (n=31) or COX-1 (n=9) as determined using the Cytoscape network were examined as separate groups for significant differences between healthy controls and APS patients using Mann-Whitney U, * $p < 0.05$, ** p 0.01, *** $P < 0.001$.

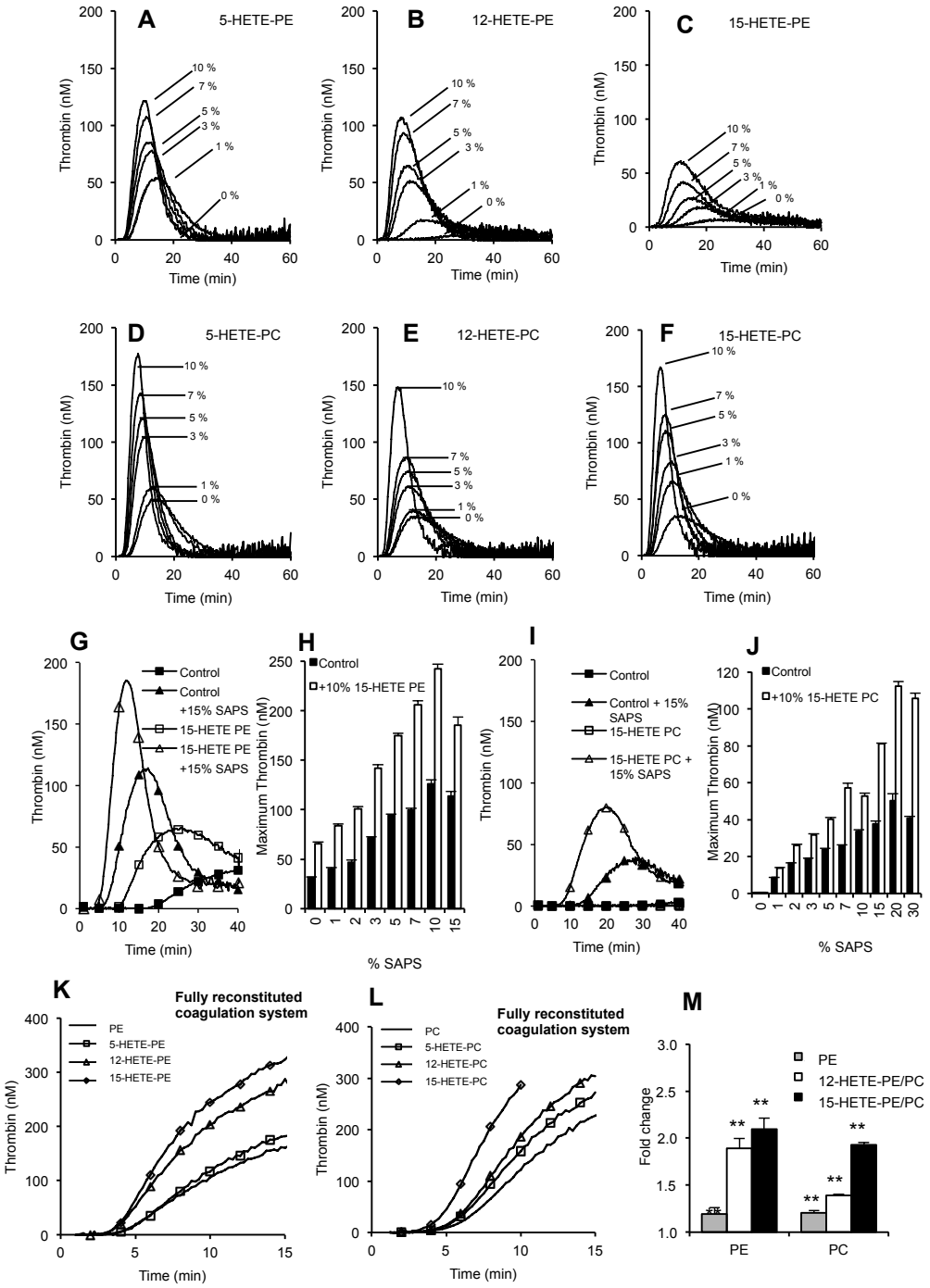

Figure 1. HETE-PE/PCs dose dependently enhance TF-dependent thrombin generation through a PS-dependent mechanism. Thrombin generation was initiated by addition of liposomes to pooled platelet poor plasma (PPP) as described in Methods, using a thrombinoscope. *Panels A-C. HETE-PEs enhance TF-dependent coagulation in plasma.* Liposomes contained 10 pM recombinant TF with 65 % DSPC, 5 % SAPS and 30 % SAPE, with 0 – 10 % SAPE replaced with 0 – 10 % HETE-PE. *(A)* 5-HETE-PE, *(B)* 12-HETE-PE, *(C)* 15-HETE-PE. *Panels D-F. HETE-PCs enhance TF-dependent coagulation in plasma.* Liposomes contained 10 pM TF, 55 % DSPC, 5 % SAPS, 30 % SAPE, with 0 – 10 % SAPC replaced with < 10 % HETE-PC. *(D)* 5-HETE-PC, *(E)* 12-HETE-PC, *(F)* 15-HETE-PC. Representative traces are shown of experiments repeated at least 3 times. *Panels G-J. 15-HETE-PE/PC enhances PS-dependent thrombin generation.* Pooled PPP was activated using liposomes, as above, where SAPE was replaced with 15-HETE-PE/PC, with/without SAPS (replacing PC) as indicated on the figure. Representative traces (Panel G, I) and maximum thrombin at varying PS concentration (Panel H, J) are shown (n = 3 runs, mean ± SEM). *Panels K-M. HETE-PE/PCs promote activities of coagulation factors in a full reconstitution system.* Thrombin generation was initiated by addition of liposomes to purified factors II, V, VII, VIIII, IX, X at physiological concentrations, as described in Methods. Liposomes contained *(Panel K)* 65 % DSPC, 5 % SAPS, 30 % SAPE, with 10 % SAPE (control) or 10 % HETE-PE or *(Panel L)* 55 % DSPC, 5 % SAPS, 30 % SAPE, 10 % SAPC (control) or 10% HETE-PC. Panel M shows summary data showing fold-change for the maximum thrombin generation rate observed (slope of lines in K,L) for each isomer (n = 3 runs, mean ± SEM). ** $p<0.01$, * : $p<0.05$, single-factor ANOVA and post-hoc Tukey tests.

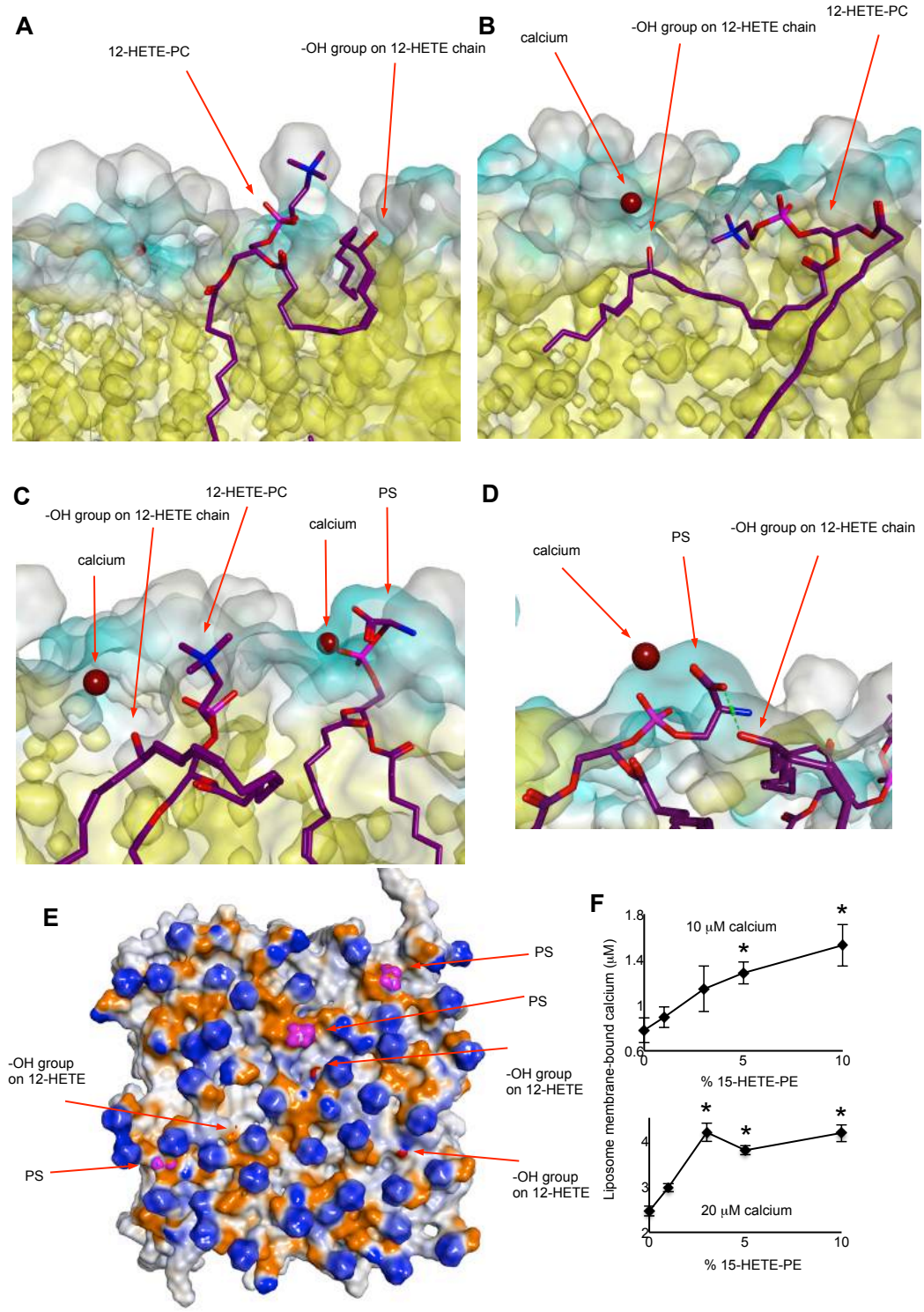

Figure 2. Molecular dynamics simulation demonstrates association of the HETE-PL hydroxyl group with the polar environment, serine and calcium ions, while HETE-PL membranes bind more calcium. *Panels A-E. Molecular dynamics shows HETE –OH group altering membrane behavior.* Molecular simulations were undertaken for 300 ns using 5% SAPS, 5% SAPC, 30% SAPE, 55% DOPC, 5% 12-HETE-PC as described in Methods. *Panels A-D*. Side views showing hydrophobic (yellow), charged phosphate groups (cyan) and PC headgroups (grey). Note bending of HETE with association of –OH groups with membrane surface (Panels A), as well with calcium (Panel B,C) and the PS headgroup (Panel D). *Panel E.* Top view looking down on membrane showing areas of positive charge (blue), negative charge (brown), PS headgroups (pink) and HETE hydroxyl groups (red). Note that all three PS and HETE –OH groups are visible (labeled) from above. *Panel F. Binding of calcium to membranes is increased by 15-HETE-PE.* Liposomes comprising 65 % DSPC, 30 % SAPE, and 5 % SAPS, with up to 10 % SAPE replaced by 15-HETE PE were tested for calcium binding using by Fluo-FF fluorescence, as described in Methods. **p<0.01 and *p<0.05 show significance compared to no added 15-HETE PE (n = 3 separate samples, mean ± SEM).

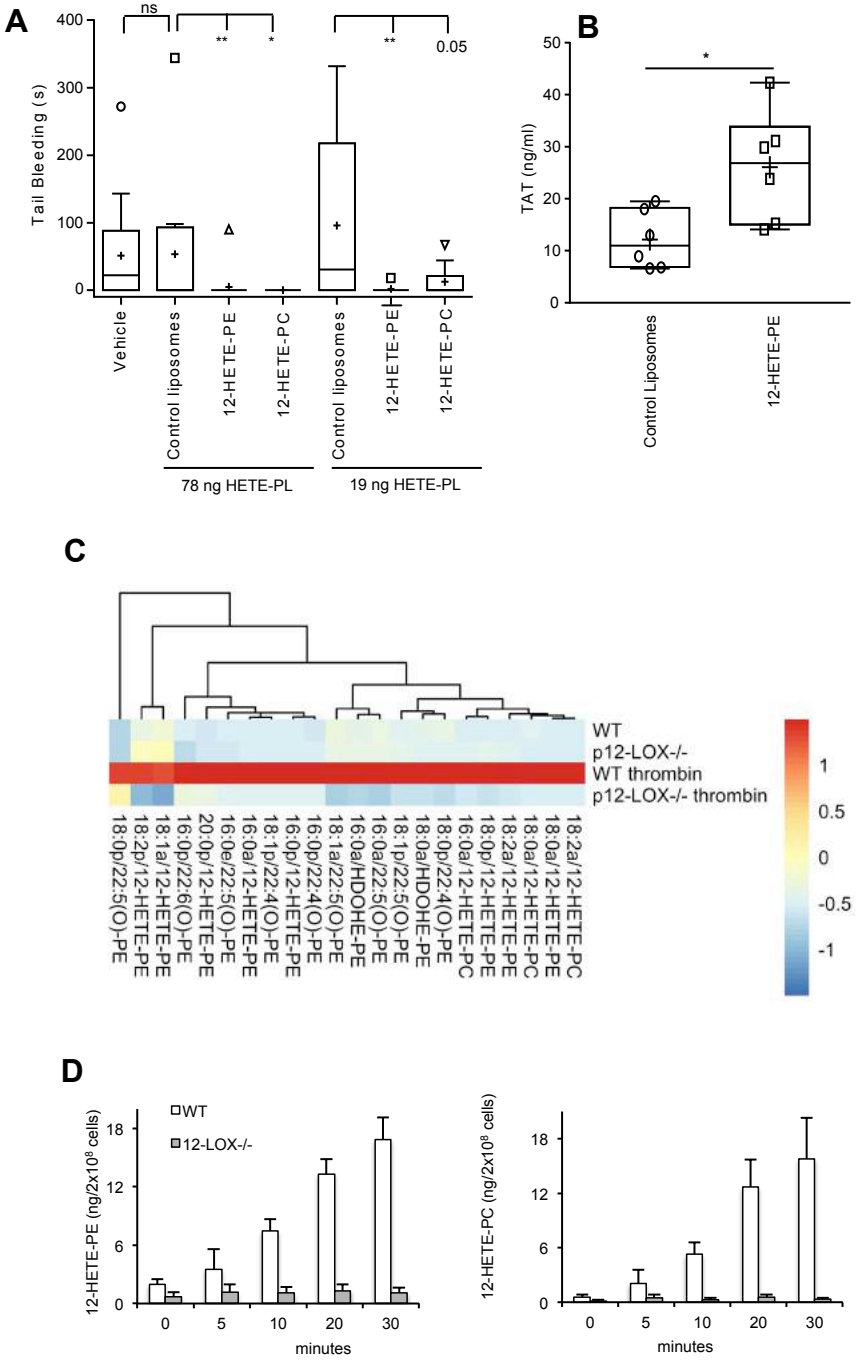

Figure 3. HETE-PL liposomes prevent tail bleeding and elevate TAT levels *in vivo,* while platelets from mice genetically lacking p12-LOX fail to generate numerous eoxPL. *Panel A 12-HETE-PE/TF intra-dermal administration prevents tail bleeding in adult mice.* 11-week old male C57BL/6J mice were injected with liposomes containing TF with or without 12-HETE-PE or -PC, immediately proximal of a tail cut, and bleeding time and blood loss recorded as in Methods (n = 10 - 16 mice per group). ** $p \leq 0.01$, * $p \leq 0.05$. Mann Whitney U test *Panel B. 12-HETE-PE elevates thrombin-anti-thrombin (TAT) complexes in vivo.* Control or HETE-PE-containing liposomes were injected i.v. into wild type mice and plasma obtained after 1 hr. TAT levels were measured using ELISA as described in Methods (n = 6 mice per group, * $p \leq 0.05$). *Panel C. Murine washed platelets generate several eoxPL on thrombin activation, that are absent in p12-LOX-deficiency.* Murine washed platelets were activated for 30 min using 0.2 U/ml thrombin, then lipids extracted and analyzed for eoxPL as described in Methods (n = 3, mean). Heatmap was generated as described in Methods using the pheatmap package in R. *Panel D. Time course of generation of 12-HETE-PEs and –PCs shows lipids continue to elevate up to at least 30 min post activation.* Platelets from wild-type or 12-LOX$^{-/-}$ mice (2 x 10^8/ml) were activated using 0.2 U/ml human thrombin for 0 - 30 min at 37 °C, and lipids then extracted and quantified as described in Methods. HETE-PE represents the sum of 16:0p/12-HETE-PE, 18:1p/12-HETE-PE, 18:0/12-HETE-PE, and 18:0a/HETE PE. HETE-PC represents the sum of 16:0a/12-HETE-PC and 18:0a/12-HETE-PC (mean ± SEM, n = 8 mice).

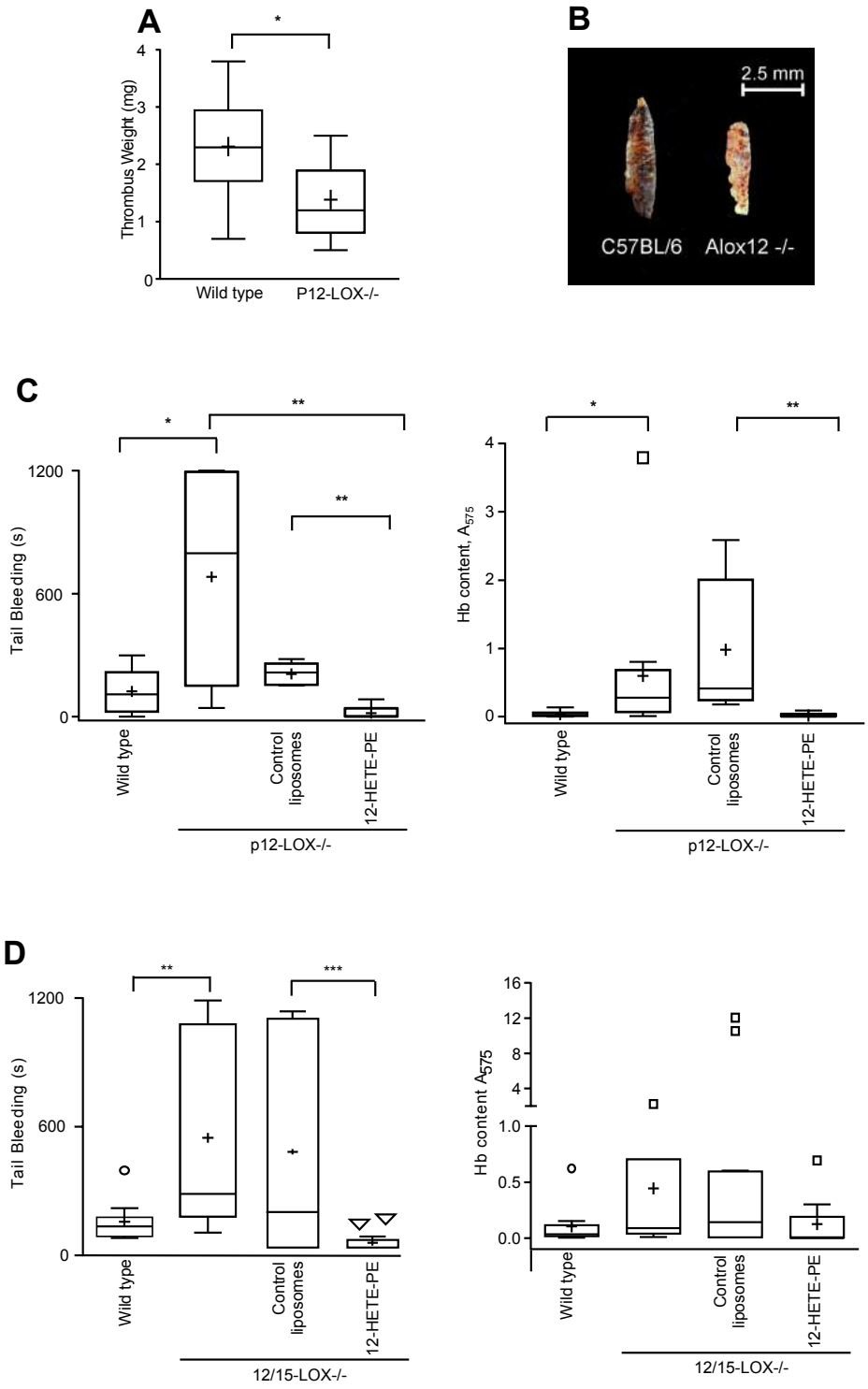

Figure 4. Mice lacking either 12/15- or p12-LOX have impaired venous coagulation in vivo, that can be restored using 12-HETE-PE liposome administration. *Panels A,B. p12-LOX deficient mice show lower thrombus formation in vivo following challenge.* Venous thrombosis was induced *in vivo* in p12-LOX$^{-/-}$ mice as described in Methods (n = 7-9 mice per group). A representative thrombus is shown. *Panel C. p12-LOX deficient mice have impaired hemostasis in vivo.* 8-11 week old male wild type C57BL/6J or p12-LOX$^{-/-}$ mice were administered a tail cut, and bleeding time and blood loss recorded as in Methods. Liposomes containing 19 ng 12-HETE-PE or control liposomes were administered in 10 ml PBS, just upstream of the cut, and immediately beforehand (n = 6 – 12 mice per group ** $p \leq 0.01$). *Panel D. 12/15-LOX deficient mice have impaired hemostasis in vivo.* As for Panel C, 8 - 11 week old male wild type C57BL/6J or 12/15-LOX$^{-/-}$ mice were administered a tail cut with/without liposomes, and bleeding time and blood loss recorded as in Methods (n = 12 – 19 mice per group, ** $p \leq 0.01$), Mann Whitney U test .

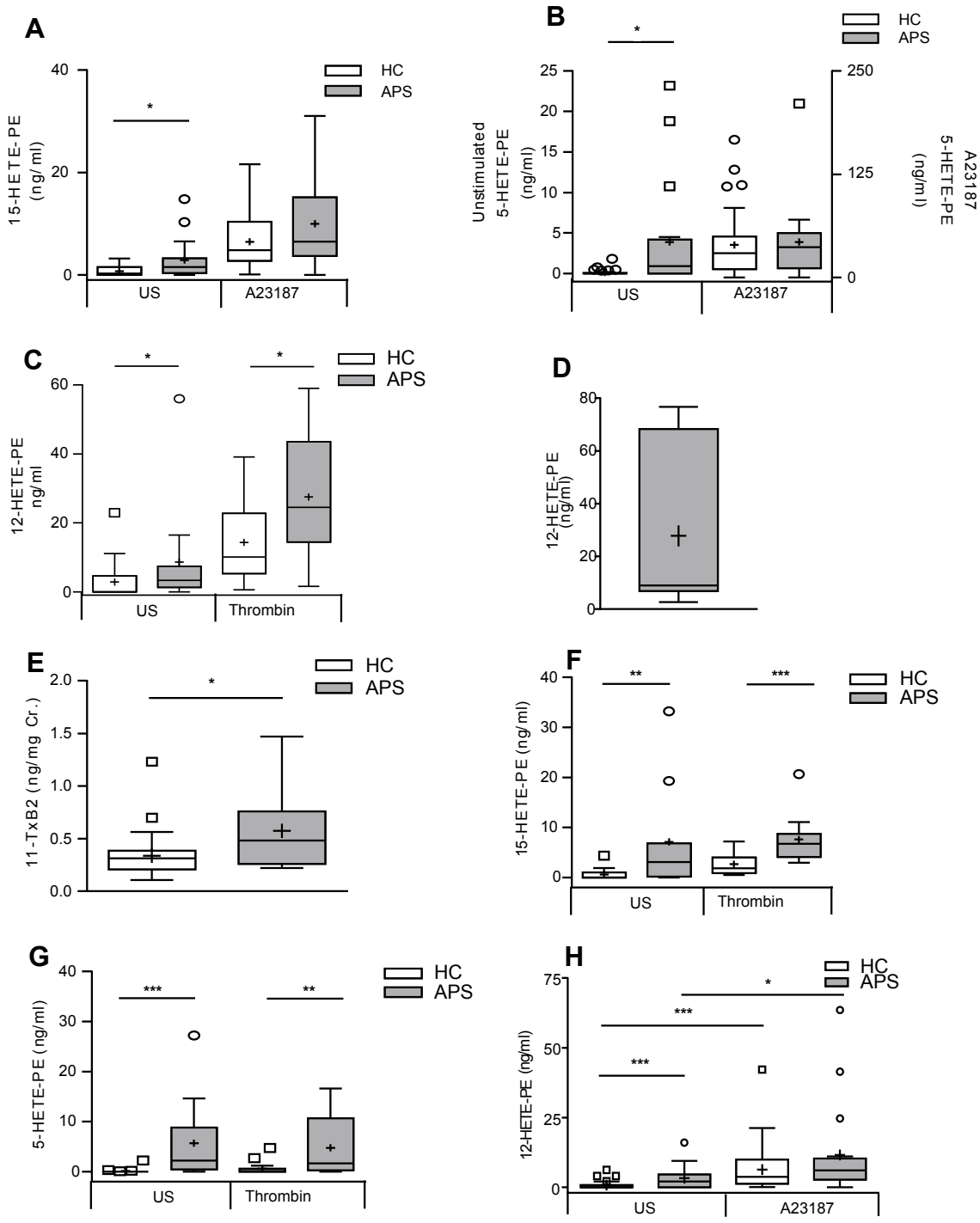

Figure 5. HETE-PEs are elevated in APS leukocytes and platelets. HETE-PEs were quantified as individual molecular species then combined. *Panels A,B. 15- and 5-HETE-PEs are elevated in leukocytes from APS patients.* Total leukocytes isolated as described, were stimulated at 4 x 10^6 cells/ml with 10 μM A23187 for 30 mins at 37 °C, then lipids analyzed for HETE-PEs as described in Methods (n = 34 (HC, Healthy controls), 17 (APS) people). *Panel C. 12-HETE-PEs are elevated in APS platelets*. Washed platelets were isolated and stimulated with 0.2 U/ml thrombin for 30 min at 37 °C as described in methods (n = 18 (HC), 12 (APS) people). *Panel D. APS platelets that spontaneously aggregated contain high levels of 12-HETE-PEs*. During the final washing step, a number of APS platelet isolates spontaneously aggregated (n = 7 patients). Lipids were extracted and analyzed for 12-HETE-PEs as in Methods. *Panel E. Urinary TXB_2 is elevated in APS*. Urine was extracted as described in Methods before GC/MS analysis as described in Methods (n = 32 (HC), 9 (APS)). *Panels F,G. Leukocyte-derived 15- and 5-HETE-PEs are elevated basally in APS platelets*. Platelets were prepared as in Panel C, then analyzed for HETE-PEs (n = 18 (HC), 12 (APS) people). *Panel H. Platelet derived 12-HETE-PEs are elevated basally in APS leukocytes*. Total leukocytes were isolated and stimulated at 4 x 10^6 cells/ml with 10 μm A23187 for 30 min at 37°C and then analyzed for 12-HETE-PEs as described in Methods (n = 34 (HC), n = 18 (APS) people), (*** $p \leq 0.001$, ** $p \leq 0.01$, * $p \leq 0.05$), Mann Whitney U test .

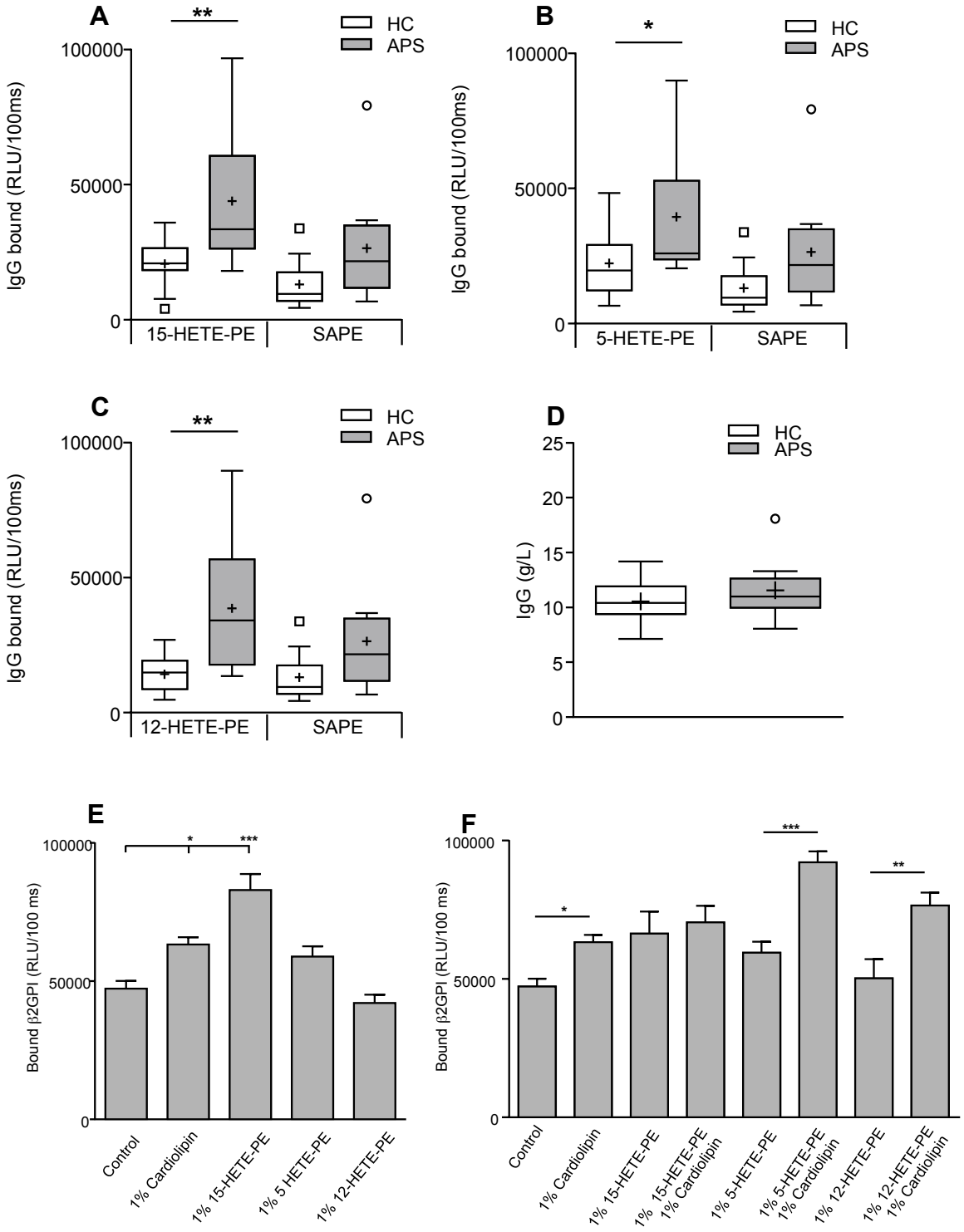

Figure 6. Circulating IgG against HETE-PEs are elevated in APS and β2BP1 binding to membranes is enhanced by HETE-PEs *Panels A-C. IgG against HETE-PEs are significantly elevated in APS plasma.* Levels of IgG antibodies to HETE-PEs were determined by diluting plasma 1:12 and testing binding to the indicated antigens as described in Methods. SAPE was used as unoxidized lipid comparison. All samples were analyzed in triplicate (n = 18 (HC), n = 9 (APS) people). * $p < 0.05$, ** p 0.01, Mann Whitney U test *Panel D. IgG titers are comparable in healthy control and patient plasma.* Total IgG was determined in plasma from patients with APS and healthy controls (n = 34 (HC), n = 10 (APS) people). *Panel E. HETE-PEs enhance β2GPI binding to lipid membranes.* Binding of β2GPI to liposomes in the presence of cardiolipin or 15-HETE-PE, 5-HETE-PE or 12-HETE-PE alone was determined as described in Methods. *Panel F. HETE-PEs enhance cardiolipin-dependent β2GPI binding to lipids.* Binding of β2GPI to liposomes in the presence of cardiolipin with/without 15-HETE-PE, 5-HETE-PE or 12-HETE-PE was determined as in Panel E. For Panels D,E, n = 3 separate experiments, each in triplicate. mean ± SEM. Significance was determined using one-way ANOVA, Tukey-Kramers test * $p < 0.05$, ** p 0.01, *** P <0.001.

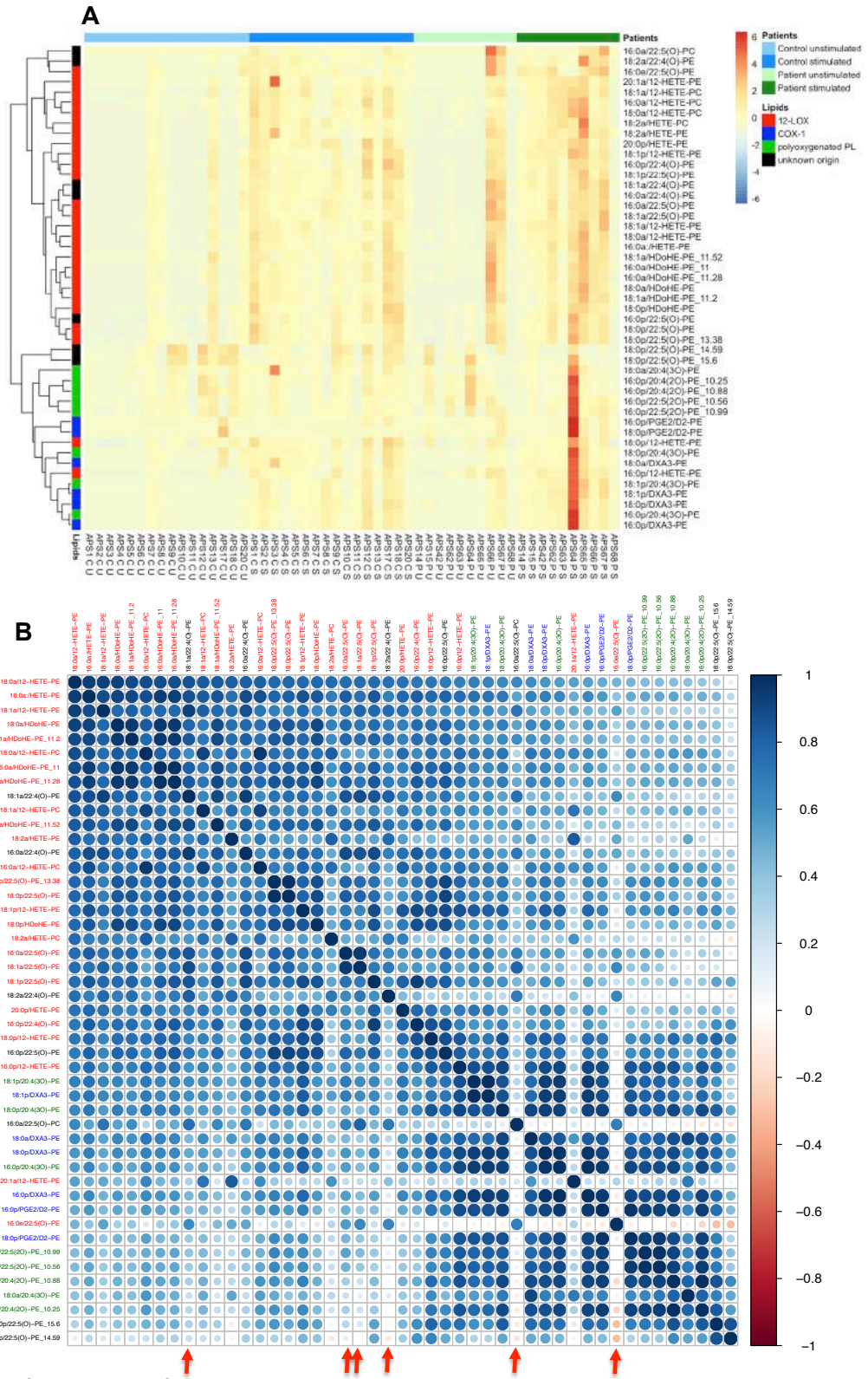

Figure 7. Lipidomic profiling of 47 eoxPL defines their enzymatic origin and regulatory networks. Washed platelets were isolated from healthy controls or APS patients and activated using thrombin (0.2 U/ml, 30 min) before lipid extraction and analysis using LC/MS/MS for 47 eoxPL as described in Methods (n = 16 HC, 10 APS people). *Panel A. p12-LOX and COX-1 derived lipids cluster into distinct families based on Sn2 fatty acid composition*. A heatmap showing effect of thrombin on individual lipid levels was generated using the pheatmap package in R using hierarchical clustering (complete linkage method) to group similar lipids. *Panel B. Plotting correlation between individual lipids illustrates additional relatedness between families of ions.* Correlations between lipids across the whole cohort were plotted in a grid, in order of decreasing correlation with 18:0a/12-HETE-PE, as described in Methods. Red: p12-LOX, blue: COX-1, green: polyoxygenated PL, black: unknown origin. Red arrows identify a group of 6 lipids (almost all acyl with 22:5(O) or 22:4(O) at *Sn2*) that correlate as a group suggesting relatedness.

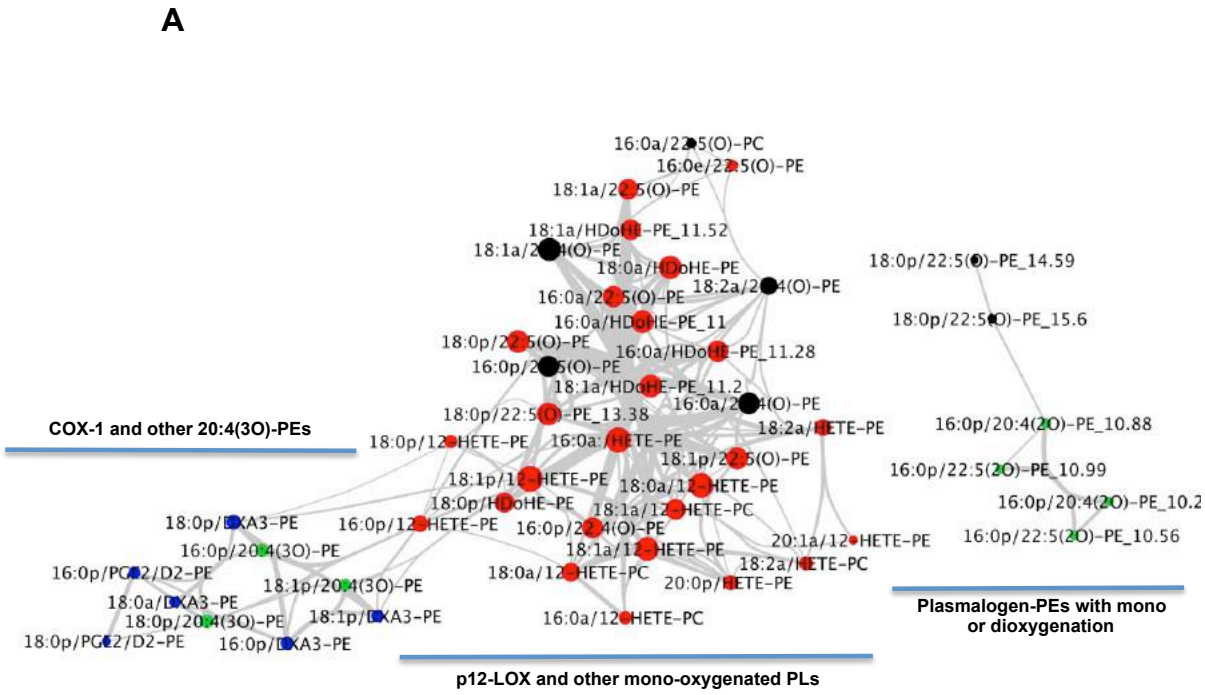

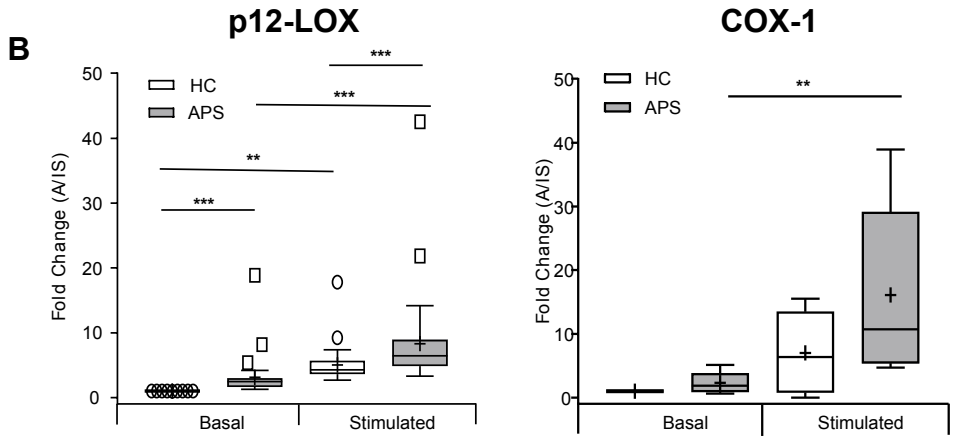

Figure 8. Cytoscape network confirms enzymatic origin of lipids, and identifies an additional group regulated independently of known pathways, and p12-LOX derived eoxPL are significantly elevated in APS platelets. *Panel A. A Cytoscape network correlation identifies three groups of eoxPL*. Cytoscape 1.2.3 correlation was performed (correlation > 0.8) using data shown in Figure 7A, with nodes as individual lipids and degree (size) determined by number of links to others. Edge thickness represents correlation between individual nodes. Lipids were identified as COX-1 or p12-LOX derived based on aspirin sensitivity or their absence in p12-LOX$^{-/-}$ mice, as described in Results. *Panel B. p12-LOX lipids are significantly elevated in APS, as a group either with/without thrombin activation.* Platelet lipids identified as originating from p12-LOX (n=31) or COX-1 (n=9) as determined using the Cytoscape network were examined as separate groups for significant differences between healthy controls and APS patients using Mann-Whitney U, * $p < 0.05$, ** p 0.01, *** P <0.001.

Supplementary Methods and Data

Supplementary Methods

Materials. Corn trypsin inhibitor (CTI, recombinant), and full length tissue factor (TF, human recombinant) were from Haematologic Technologies Inc*).* FII Fluorogenic substrate (Z-Gly-Gly-Arg-AMC) was from Bachem (St Helens, UK). T-cal Thrombinoscope calibrator was from Stago. 1-Stearoyl-2-arachidonoyl-phosphatidylethanolamine, -phosphatidylcholine and -phosphatidylserine (SAPE, SAPC, SAPS) and 1,2-di-stearoyl-phosphatidylcholine (DSPC) were from Avanti Polar Lipids. 2,2'-Azobis(4-methoxy-2,4 dimethyl-valeronitrile) (MeOAVM) was from WAKO. All other chemicals and lipsofast membranes were from Sigma-Aldrich, except N-methyl Benzohydroamic acid (NMBHA), synthesized in-house according to (1). Solvents were from Fisher Scientific*.*

Study approvals and patient demographics

Patients (total 18) with APS associated with venous thrombosis were recruited from haematology clinics. All had at least one incidence of venous and/or arterial thrombosis and tested positive for at least one laboratory criterion (Lupus anti-coagulant and/or high anti-cardiolipin IgG titres and/or high anti-β2GPI IgG titres measured on two occasions at least 12 weeks apart). Patients were not taking aspirin, or other non-steroidal anti-inflammatory drugs at the time of venepuncture. Most were taking anti-coagulants, e.g. warfarin or rivaroxiban, none had diabetes, and only one had high cholesterol at time of sampling. Full details on all patients is in Supplementary Table 1, below. Blood

samples were collected from patients following a routine clinical visit, in a quiescent state with no clinical thrombotic episode at the time of sampling. Healthy controls (total 34) were recruited from the local population, and were excluded if they had a history of arterial or venous thrombosis, recurrent fetal loss, cardiac disease or any other chronic inflammatory diseases such as rheumatoid arthritis, SLE, diabetes, high cholesterol, abnormal renal or liver function, or other diseases that may conflict with the study parameters. Individuals within the HC group had not taken aspirin, non-steroidal anti-inflammatory drugs or any other medication in the preceding 14 days. Informed consent was obtained from all participants. Age and gender demographics is given in Table Blood samples were collected from APS patients and healthy controls via venepuncture from the median cubital vein. Full blood counts (FBC) were collected, any patients or healthy controls with an abnormal FBC at the time of sample collection were retrospectively omitted from the study. Washed platelets and leukocytes were isolated and activated as described. Serum, plasma and urine was collected as described.

Patient	Age	Gender	AT	VT	Chol	DM	medications relevant to vascular disease
APS014	27	F	N	Y	N	N	warfarin, hydroxychloroquine
APS015	22	F	N	Y	N	N	warfarin
APS029	43	F	Y	Y	N	N	warfarin, hydroxychloroquine
APS030	52	F	Y	Y	N	N	warfarin
APS032	79	M	N	Y	Y	N	warfarin, propranolol
APS033	31	F	Y	Y	N	N	rivaroxiban
APS040	51	M	N	Y	N	N	warfarin, losartan
APS042	39	F	Y	N	N	N	warfarin
APS044	35	M	N	Y	N	N	warfarin, amlodipine, bendroflumethiazide, doxazosin
APS060	47	F	Y	Y	N	N	warfarin, lanzoprazole, lisinopril, amlodipine
APS061	58	F	N	Y	N	N	None
APS062	75	F	N	Y	N	N	warfarin
APS063	36	F	N	Y	N	N	rivaroxiban
APS064	41	M	N	Y	N	N	rivaroxiban
APS065	38	F	N	Y	N	N	rivaroxiban
APS066	33	F	N	Y	N	N	enoxaparin
APS067	55	F	N	Y	N	N	warfarin
APS068	58	F	N	Y	N	N	rivaroxiban

Supplementary Table 1. Patient demographics. AT: arterial thrombosis, VT: venous thrombosis, Chol: cholesterol lowering medication, DM: Diabetes Mellitis

	APS Participant	Healthy Control
Male	n = 4	n = 15
Female	n = 14	n = 19
Mean Age ± St Dev	45.6 ± 15.4	36.2 ± 9.2
Median Age	42	33

Supplementary Table 2. Age and gender demographics of study participants

Liposome composition for β2GP1 binding experiments: All liposomes were as described above after extrusion, but with the following lipid composition: 55% distearoly-PC (DSPC), 15 % stearoyl-arachidonyl-PS (SAPS), 10 % stearoyl-arachidonyl-PC (SAPC), 1 % stearoyl-arachidonyl-PE-biotin (SAPE-B, generated by reacting NHS-biotin with PE and purification using HPLC), 19 % stearoly-arachidonyl-PE (SAPE). In some experiments, an equivalent amount of SAPE was replaced with 1 % 15-, 12- 5-HETE-PE, and/or 1 % cardiolipin.

Determination of circulating antibodies to HETE-PEs. Specific Ab titres to individual HETE-PEs were determined by chemiluminescent ELISA as previously described (3). Lipids were coated onto Microfluor plates at 20 μg/ml and subsequently blocked with 0.5% fish-gelatin in 0.27 mM PBS-0.27 mM EDTA. EDTA plasma samples (1:12) were diluted in PBS-0.27 mM EDTA and incubated for 1 hour at room temperature. The

bound IgG was measured using an anti-human IgG alkaline phosphatase-conjugated secondary antibody (Sigma Aldrich) and LumiPhos 530 (Lumigen, Inc). Data are expressed as the relative light units per 100 ms (RLU/100 ms).

Isolation of human leukocytes. Leukocytes were isolated from 20 ml citrate anticoagulated whole blood. Briefly, 20 ml of whole blood was mixed with 4 ml of 2 % citrate and 4 ml of Hetasep (Stem Cell Technologies) and allowed to sediment for at least 45 minutes. The upper plasma layer was recovered and centrifuged at 250 g for 10 min at room temperature. The pellet was resuspended in ice-cold 0.4 % trisodium citrate/PBS and centrifuged at 250 g for 5 min at 4 °C. Erythrocytes were removed by hypotonic lysis. Leukocytes were resuspended in Krebs buffer at 4 x 10^6/ml. Leukocytes were activated at 37 °C with 10 μM A23187 in the presence of 1 mmol/$CaCl_2$, for 30 min, prior to lipid extraction.

Isolation of serum, plasma and urine. Blood was collected into EDTA, Lithium-Heparin, or Citrate vacutainers prior to centrifugation at 900 g. The plasma layer was collected and centrifuged again at 900 g to remove any residual platelets. Plasma was stored at -80 °C for use in *in vitro* assays. Whole blood was collected into a clot-activating vacutainer and centrifuged at 900 g. The serum was collected and centrifuged again at 900 g to remove any residual cells. Serum was stored at -80 °C for use in *in vitro* assays. Urine was collected into universal containers, samples were aliquoted and stored at -80 °C until use.

Isolation and activation of mouse washed platelets. Mouse blood was obtained by cardiac puncture directly into a syringe containing 150 μl ACD (2.5% w/v trisodium

citrate, 1.5 % w/v citric acid, 100 mM glucose). The syringe was emptied into an eppendorf containing 150 μl 3.8 % w/v sodium citrate, and 300 μl of modified Tyrode's buffer was then added (145 mM NaCl, 12 mM $NaHCO_3$, 2.95 mM KCl, 1 mM $MgCl_2$, 10 mM HEPES, 5 mM Glucose). The blood was spun for 5 min at 150g at 25°C, and platelet-rich-plasma (PRP) removed. Another 400 μl of Tyrode's buffer was added, carefully mixed into the blood without inverting the tube, and more PRP removed after a second, identical, spin. A third spin at 530 g for 5 min on the pooled PRP pelleted the platelets, plasma was removed, and the platelets were re-suspended in Tyrode's buffer at 2 x 10^8 ml^{-1}. Half the platelets were used as unstimulated controls, and the rest were activated with 0.2 U/ml thrombin and 1 mM $CaCl_2$ followed by gentle mixing every 2 - 3 min for 30 min at 37 °C.

Quantification of blood loss from tail bleeding assays. C57/BL6 wild type (Charles River), 12/15-$LOX^{-/-}$ and p12-$LOX^{-/-}$ mice bred in-house were kept in constant temperature cages (20 – 22 °C) and given free access to water and standard chow. Tail bleeding assays and breeding of mice was performed under Home Office Licence PPL/3150. Male mice (11 week old) were anesthetized using 5 % isoflurane and maintained with 2 % isoflurane. Where administered, liposomes (10 ml generated as described above, using either (i) 30 % SAPE, 65 % DSPC, 5 % SAPS, and 2.5 nmol/L TF, or (ii) 20 % SAPE, 65 % DSPC, 5 % SAPS, 10 % 12-HETE-PE and 2.5 nmol/L TF) were injected immediately proximal of the cut site directly before transection of 2 - 5 mm from the distal end and immediate immersion in 37 °C physiological saline. Bleeding was observed as blood loss and time to the beginning of stable (1 min) cessation of blood flow determined, before killing *via* cervical dislocation. Blood loss was quantified by measuring the hemoglobin (Hb) content of the saline, as follows. Hemoglobin

quantitation was achieved via centrifugation of the tube at 250 x *g* for 15 min, and resuspending the red cells in 5 ml erythrocyte lysis buffer (8.3 g/L NH_4Cl, 1 g/L $KHCO_3$ and 0.037 g/L EDTA in distilled H_2O). The concentration of Hb was measured as optical density (OD) 575 nm using a UVIKON 923 double beam UV /VIS spectrophotometer (Bio-Tek Kontron Instruments) and expressed as absorbance units (AU).

Injury-related venous thrombosis. Thrombosis was induced as described previously with minor modifications (5). In brief, mice (20 - 25 g body weight) were anaesthetized with ketamin (100 mg/kg body weight) and xylazin (20 mg/kg body weight), and placed under a heating lamp to maintain constant body temperature of 37 °C. A ventral midline incision was performed and the intestines were gently put aside. The vena cava inferior was laid free carefully and a filter paper (1 mm x 2 mm x 4 mm) soaked with 4 % of aqueous ferric chloride solution was placed on top of the vessel. After 3 min, the filter paper was removed and the peritoneal cavity thoroughly rinsed with pre-warmed 0.9 % saline. After another 30 min, mice were sacrificed, blood was taken by cardiac puncture, and the vena cava containing the thrombus removed. The clot was dissected free from the vessel and prepared under a microscope for further analysis. Wet thrombus weight was measured using a precision balance (Sartorius R16P) after removal of excess water.

Liposome-β2GPI-HETE-PE binding. Liposomes were prepared by extrusion in Buffer A (20 mM HEPES, 100 mM NaCl, pH 7.4), with composition as described earlier (6). Liposomes were immobilized onto Polysorp plates (Nunc) coated with 5 μg/ml Neutravidin. 1 μg/ml β2GPI was added for 1 hour at room temperature. Bound β2GPI

was determined using anti-β2GPI-HRP antibody (1:20,000) (Cedarlane) and ECL detection (Pierce). Data is expressed as the relative light units in 100 ms (RLU/100 ms).

Lipid Bilayer Model Preparation, and membrane energy minimization and simulation protocol. A pre-equilibrated hydrate lipid bilayer consisting of 128 molecules of 1,2-Dioleoyl-sn-glycero-3-phosphocholine (DOPC), based on a previously reported study, was downloaded from the ATM database (Box ID: 30) (7,8). The lipid bilayer was structurally modified by removing DOPC using the MOE (9) builder tools according to the experimental composition of the tested liposomes to give the following composition: 5 % SAPS, 5 % SAPC, 30 % SAPE, 55 % DOPC, 5 % 12-HETE-PC. Initially, a conformational analysis of 12-HETE-PC was performed with two different low energy conformations included in the membrane. The first presented the oxidized lipid chain in an elongated structure and was used for the three 12-HETE-PCs in one monolayer. The second presented the oxidized chain in a bent conformation and was used in the other monolayer. As a result, the 12-HETE-PC presented the OH group differently on the two different membrane layers: on one side the hydroxyl groups were placed deep in the membrane, while they were close to the membrane surface on the other side. All the modified lateral chains were minimized in MOE using an OPLS-AA force field with a gradient of 0.1Kcal/mol/$Å^2$. Hydrate membrane energy minimization and simulation were performed by using Desmond (Maestro interface) with OPLS_2005 set of force field parameters (10,11). The TIP3P water model was used and the assembled system consisted of 35426 atoms enclosed in a 69 x 70 x 80 $Å^3$ triclinic box. 14 molecules of $CaCl_2$ were added as salt. Energy minimization of the system was run with a steepest descent until gradient threshold of 25 kcal/mol/Å was reached. A 300 ns MD simulation

was then performed using the Desmod default parameters with the temperature set to 300 K, pressure set at 1.01325 bar and the time step was set to 2 fs. Energy of the simulation was recorded every 120 ps, whereas the trajectory was recorded every 480 ps.

Measurement of calcium binding to membranes. Glass tubes were pre-washed using 1 M hydrochloric acid and methanol. All buffers were treated using 10 mg/ml pre-washed chelex-100 and kept in plasticware to reduce calcium contamination to 1 - 2 μM. Liposomes containing 65 % DSPC, 30 % SAPE, 5 % SAPS liposomes, or with SAPE replaced with up to 10% 15-HETE-PE were prepared in potassium phosphate buffer. Free calcium concentration in the samples was measured using 1 μM Fluo-FF calcium dye (Kd 9.7 mM, ex 485 nm, em 520 nm), with 10 or 20 μM calcium added. Decreases in free calcium in lipid solutions compared to the buffer blank represents membrane-bound calcium. A standard curve for Fluo-FF response was constructed using 10 mM nitrilotriacetic acid (Kd 78.6 μM) as calcium buffer.

i.e $[Ca^{2+}]_{membrane} = [Ca^{2+}]_{total} - [Ca^{2+}]_{free} - [Ca^{2+}]_{Fluo\text{-}FF\ bound} - [Ca^{2+}]_{contaminants}$

and for the buffer blank:

$$[Ca^{2+}]_{total} = [Ca^{2+}]_{free} - [Ca^{2+}]_{Fluo\text{-}FF\ bound} - [Ca^{2+}]_{contaminants}$$

Thrombin-Antithrombin (TAT) complex measurement. Whole blood was collected via a cardiac puncture into one-tenth volume of 3.8 % sodium citrate as an anticoagulant and centrifuged at 3,000 x g for 10 min. Plasma thrombin-antithrombin (TAT) levels were

determined using a commercially available enzyme-linked immunosorbent assay kit (Mouse Thrombin-Antithrombin Complexes ELISA Kit; ab137994, abcam).

Heatmap and Cytoscape correlation. Heatmaps were generated using the pheatmap package in R (version 3.3.1). Data was first normalised to the mean of the unstimulated control values for each lipid. Network analysis was performed with Cytoscape (version 3.4.0), utilizing pairwise correlations between lipids generated with R. The network diagram shows only correlations with a Pearson product-moment correlation coefficient value (r) > 0.8, due to the high number of interactions.

fig. S1

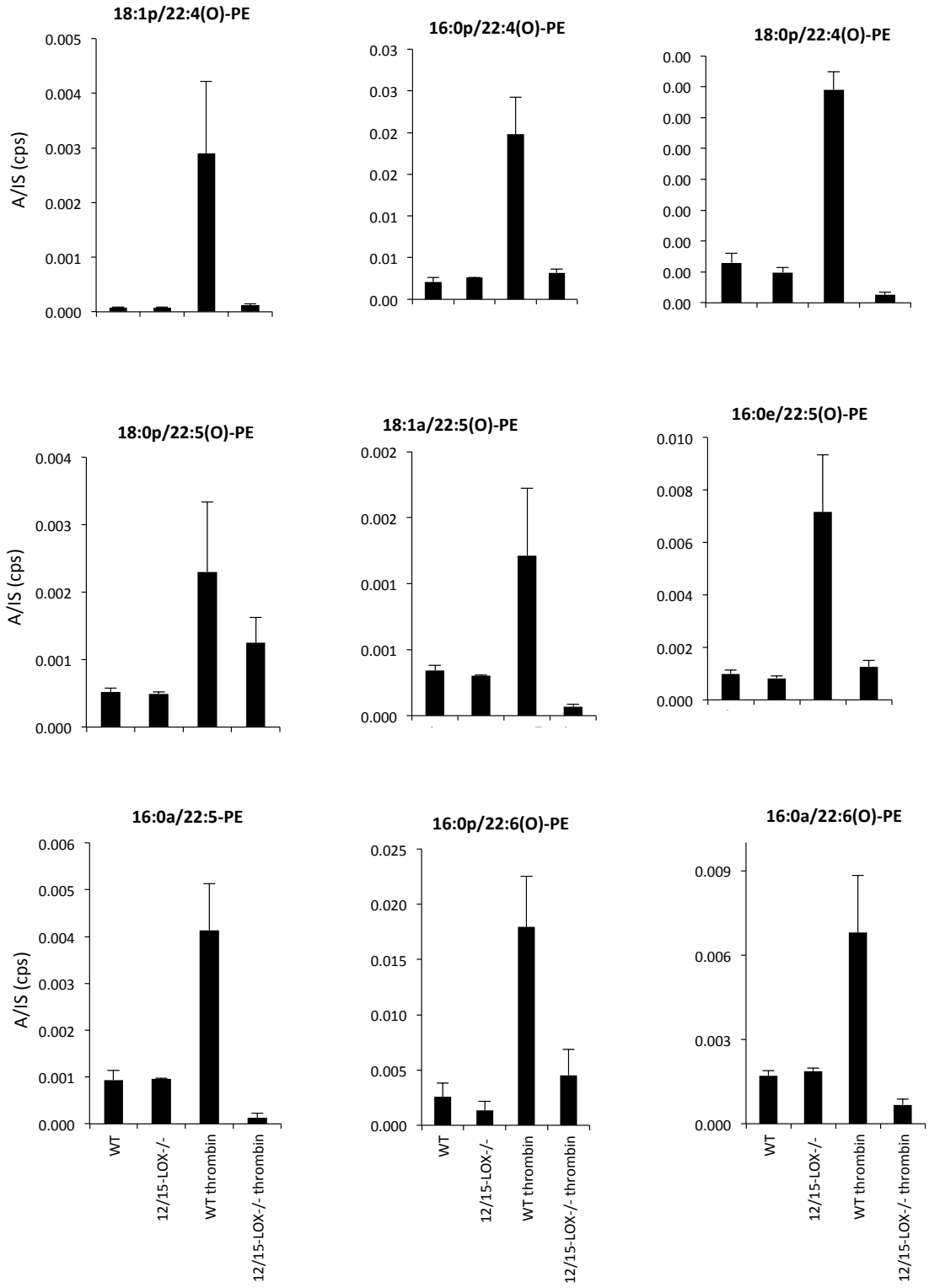
18:1p/22:4(O)-PE
16:0p/22:4(O)-PE
18:0p/22:4(O)-PE
18:0p/22:5(O)-PE
18:1a/22:5(O)-PE
16:0e/22:5(O)-PE
16:0a/22:5-PE
16:0p/22:6(O)-PE
16:0a/22:6(O)-PE
A/IS (cps)
WT
12/15-LOX-/-
WT thrombin
12/15-LOX-/- thrombin

fig. S1

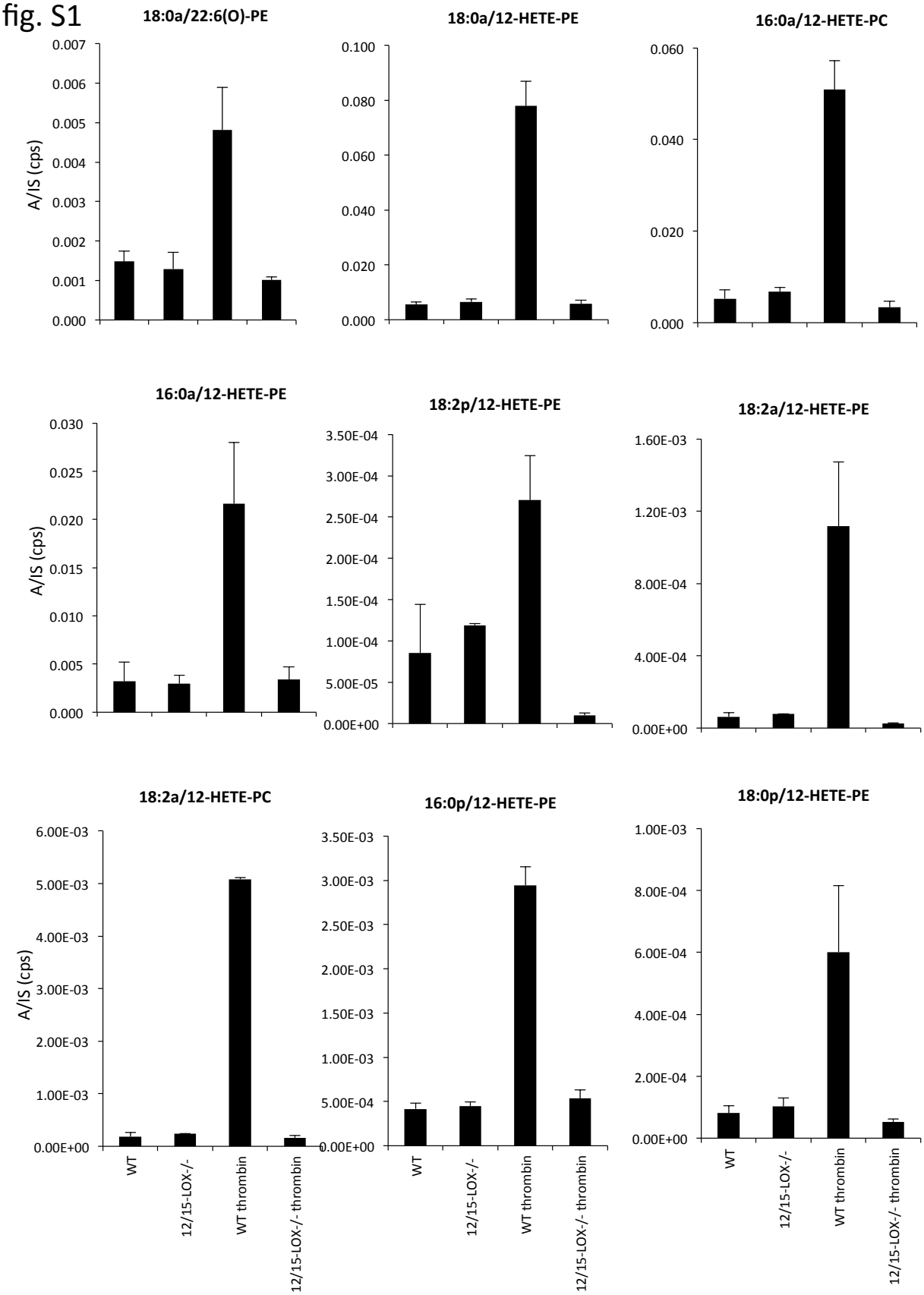
18:0a/22:6(O)-PE
18:0a/12-HETE-PE
16:0a/12-HETE-PC
16:0a/12-HETE-PE
18:2p/12-HETE-PE
18:2a/12-HETE-PE
18:2a/12-HETE-PC
16:0p/12-HETE-PE
18:0p/12-HETE-PE
A/IS (cps)
WT
12/15-LOX-/-
WT thrombin
12/15-LOX-/- thrombin

fig. S1

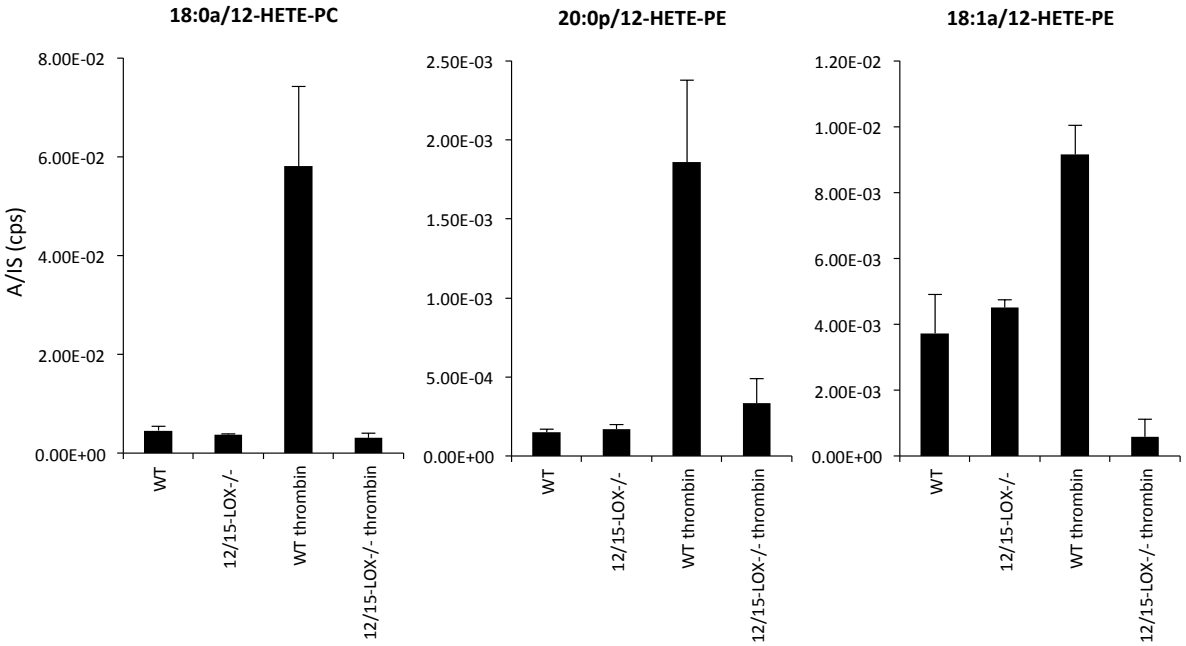

Figure S1. Primary data for generation of eoxPL by wild type and p12-LOX$^{-/-}$ washed platelets. Blood was taken by cardiac puncture and washed platelets isolated as in Methods. Platelets were activated using thrombin as outlined in Methods then analyzed for eoxPL using LC/MS/MS. Levels are expressed relative to internal standard (DMPE/DMPC) (n=3, mean +/- SEM).

fig. S2

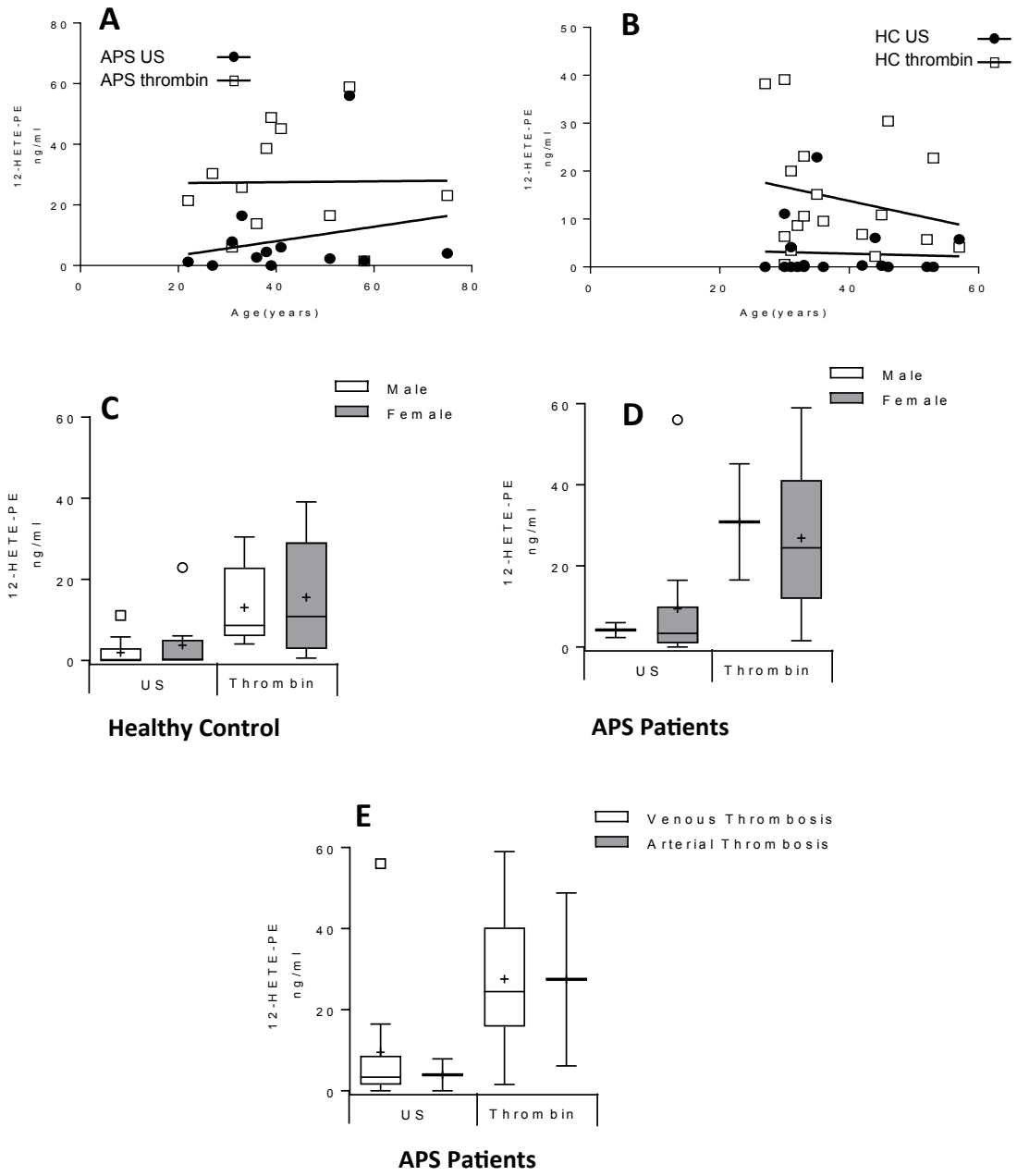

Figure S2. Analysis of HC and APS demographics for effects on eoxPL generation shows no effect of age, gender or arterial thrombosis on platelet 12-HETE-PEs. Data was analysed for platelet 12-HETE-PEs, either unstimulated (US) or following thrombin treatment, versus (A) age, APS, (B) age, HC, (C, D) gender, (E) venous vs arterial thrombosis.

fig. S3

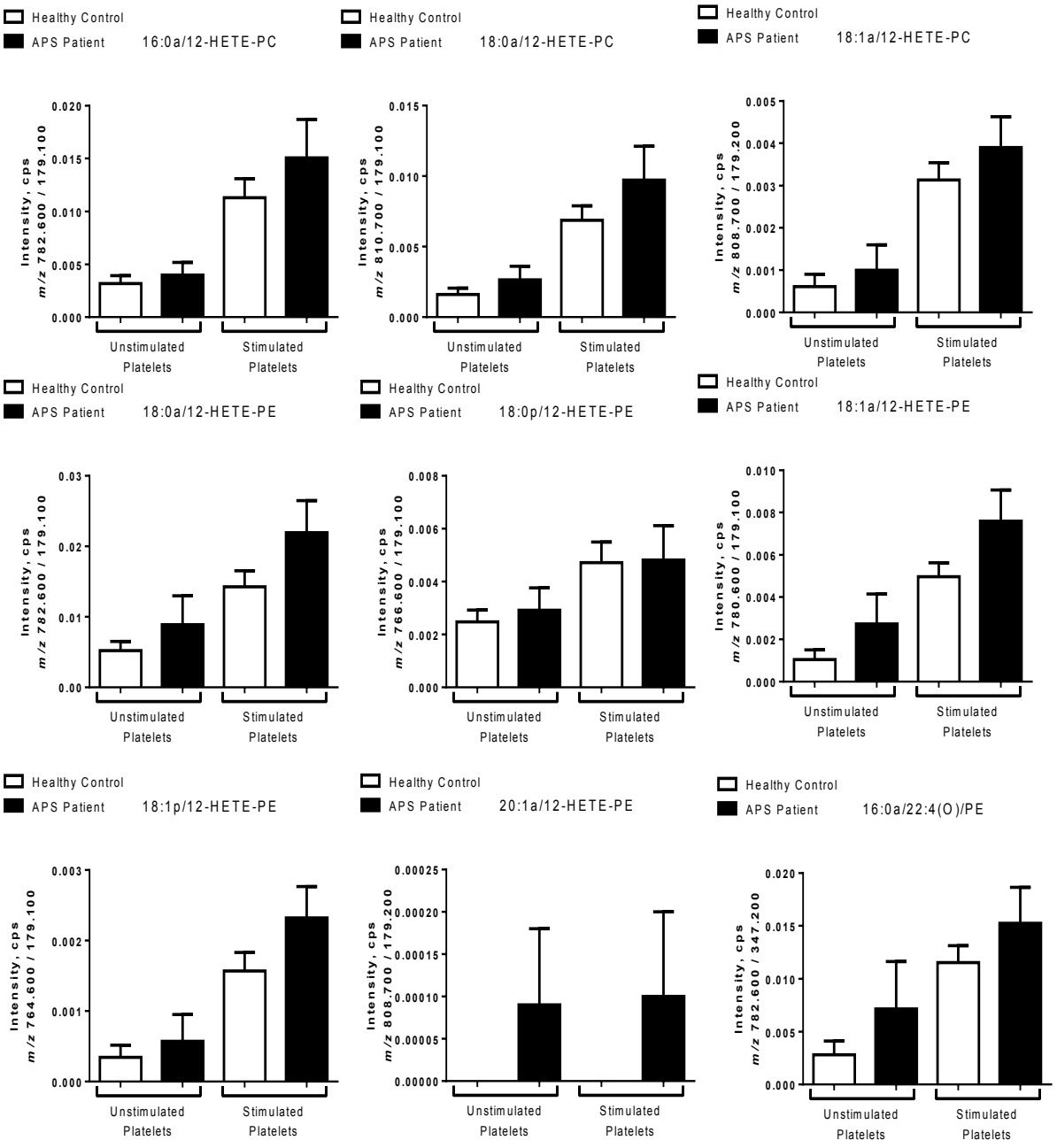
Healthy Control
APS Patient
16:0a/12-HETE-PC
18:0a/12-HETE-PC
18:1a/12-HETE-PC
18:0a/12-HETE-PE
18:0p/12-HETE-PE
18:1a/12-HETE-PE
18:1p/12-HETE-PE
20:1a/12-HETE-PE
16:0a/22:4(O)/PE
Intensity, cps
m/z 782.600 / 179.100
m/z 810.700 / 179.100
m/z 808.700 / 179.200
m/z 782.600 / 179.100
m/z 766.600 / 179.100
m/z 780.600 / 179.100
m/z 764.600 / 179.100
m/z 808.700 / 179.200
m/z 782.600 / 347.200
Unstimulated Platelets
Stimulated Platelets

fig. S3

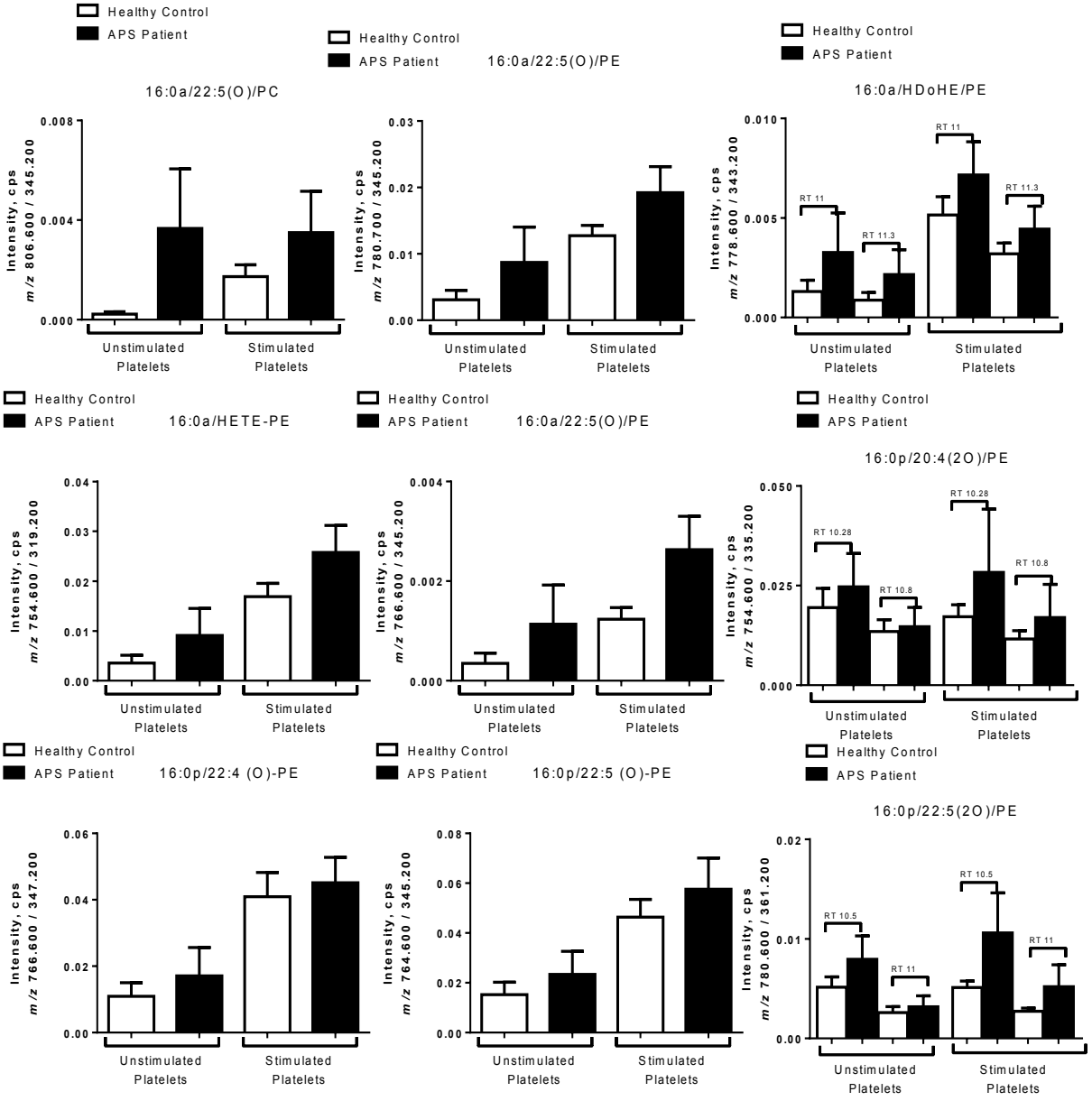
Healthy Control
APS Patient
16:0a/22:5(O)/PC
Intensity, cps
m/z 806.600 / 345.200
0.008
0.004
0.000
Unstimulated Platelets
Stimulated Platelets
16:0a/22:5(O)/PE
m/z 780.700 / 345.200
0.03
0.02
0.01
0.00
16:0a/HDoHE/PE
m/z 778.600 / 343.200
0.010
0.005
RT 11
RT 11.3
16:0a/HETE-PE
m/z 754.600 / 319.200
0.04
0.03
0.02
0.01
16:0a/22:5(O)/PE
m/z 766.600 / 345.200
0.004
0.002
16:0p/20:4(2O)/PE
m/z 754.600 / 335.200
0.050
0.025
RT 10.28
RT 10.8
16:0p/22:4 (O)-PE
m/z 766.600 / 347.200
0.06
0.04
0.02
16:0p/22:5 (O)-PE
m/z 764.600 / 345.200
0.08
0.06
16:0p/22:5(2O)/PE
m/z 780.600 / 361.200
RT 10.5

fig. S3

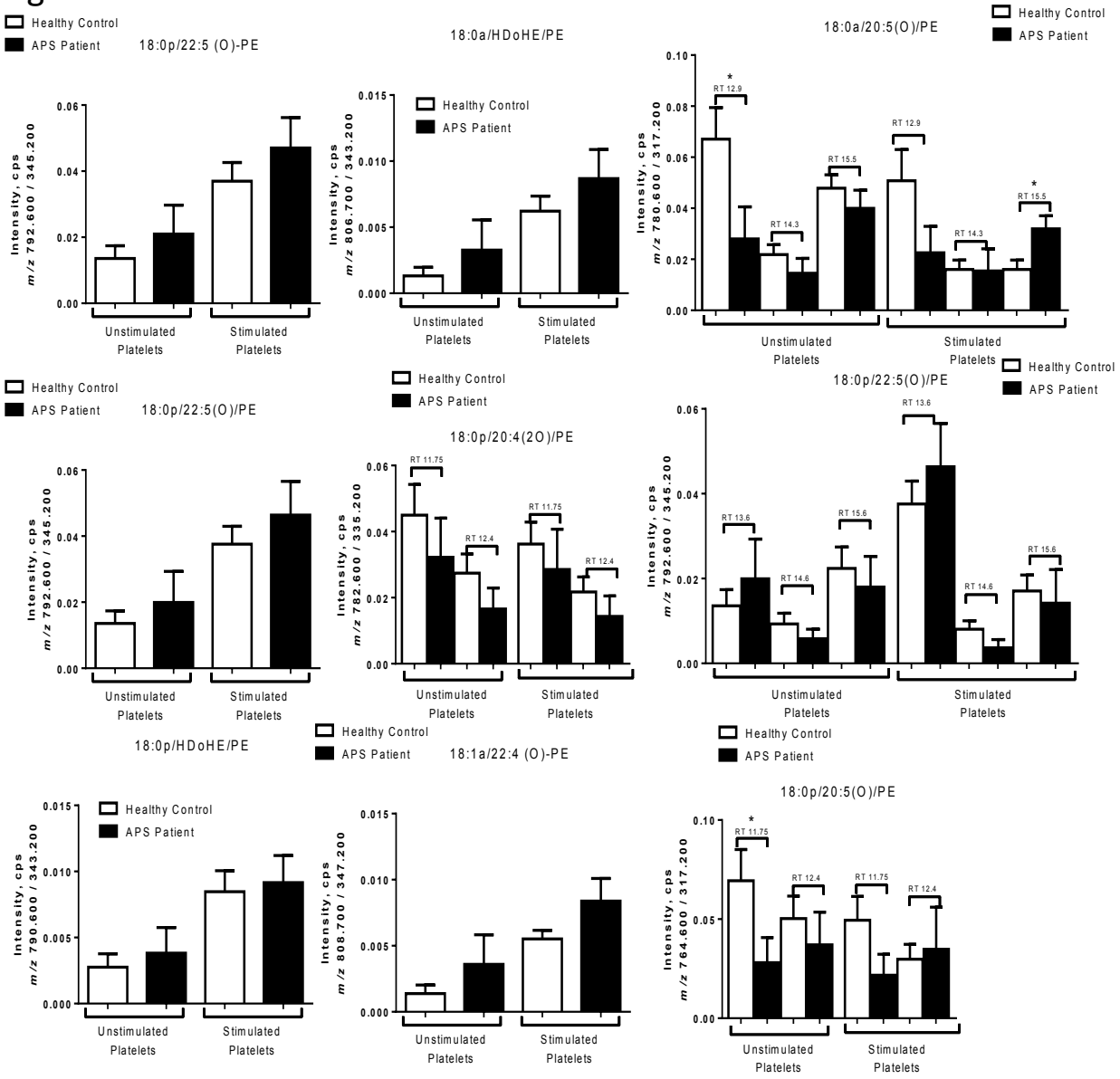
Healthy Control
APS Patient
18:0p/22:5 (O)-PE
Intensity, cps
m/z 792.600 / 345.200
Unstimulated Platelets
Stimulated Platelets
18:0a/HDoHE/PE
m/z 806.700 / 343.200
18:0a/20:5(O)/PE
m/z 780.600 / 317.200
RT 12.9
RT 15.5
RT 14.3
18:0p/22:5(O)/PE
18:0p/20:4(2O)/PE
m/z 782.600 / 335.200
RT 11.75
RT 12.4
RT 13.6
RT 14.6
RT 15.6
18:0p/HDoHE/PE
m/z 790.600 / 343.200
18:1a/22:4 (O)-PE
m/z 808.700 / 347.200
18:0p/20:5(O)/PE
m/z 764.600 / 317.200

fig. S3

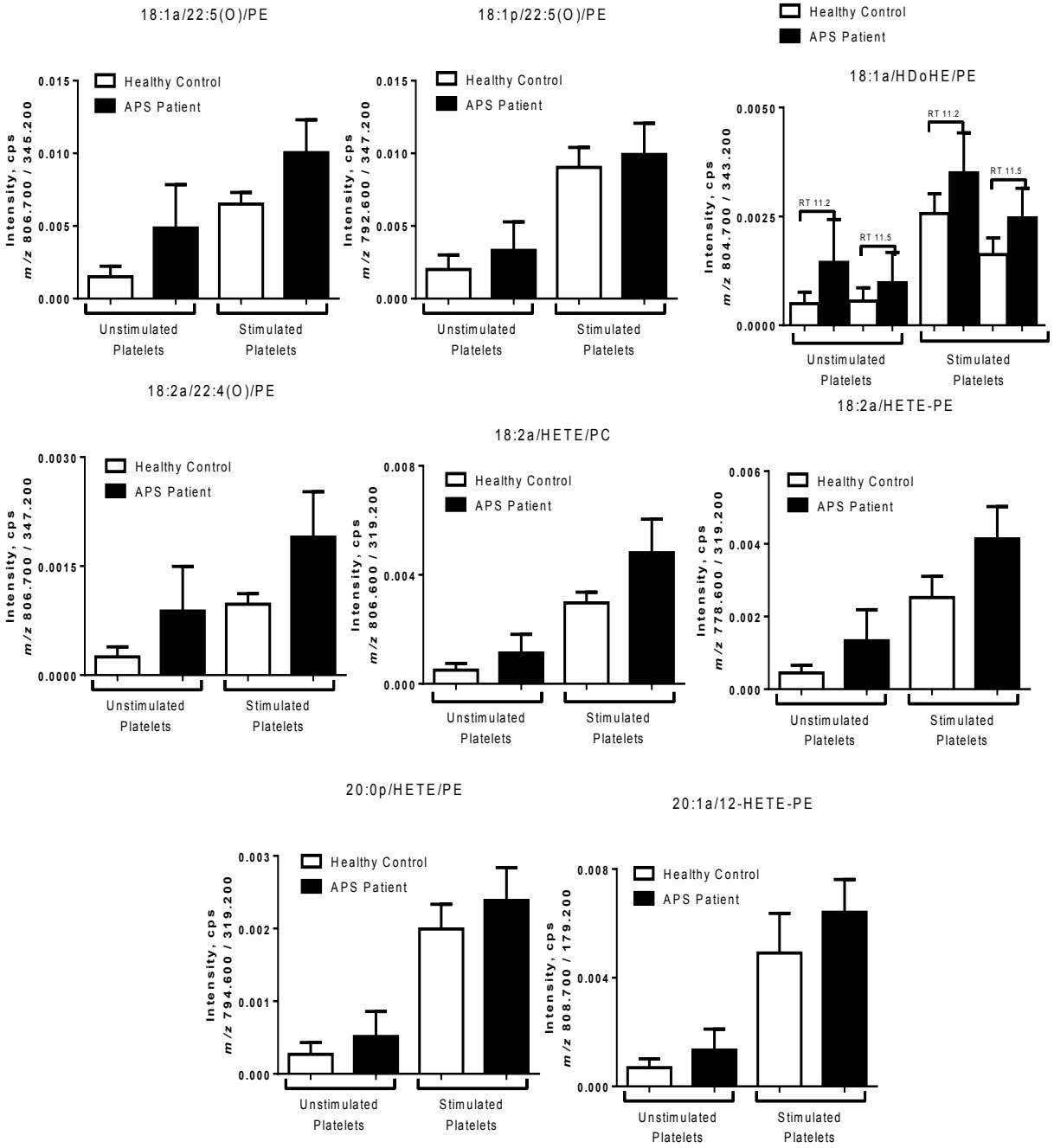
18:1a/22:5(O)/PE
18:1p/22:5(O)/PE
18:1a/HDoHE/PE
18:2a/22:4(O)/PE
18:2a/HETE/PC
18:2a/HETE-PE
20:0p/HETE/PE
20:1a/12-HETE-PE
Healthy Control
APS Patient
Intensity, cps
m/z 806.700 / 345.200
m/z 792.600 / 347.200
m/z 804.700 / 343.200
m/z 806.700 / 347.200
m/z 806.600 / 319.200
m/z 778.600 / 319.200
m/z 794.600 / 319.200
m/z 808.700 / 179.200
RT 11.2
RT 11.5
Unstimulated Platelets
Stimulated Platelets

fig. S3

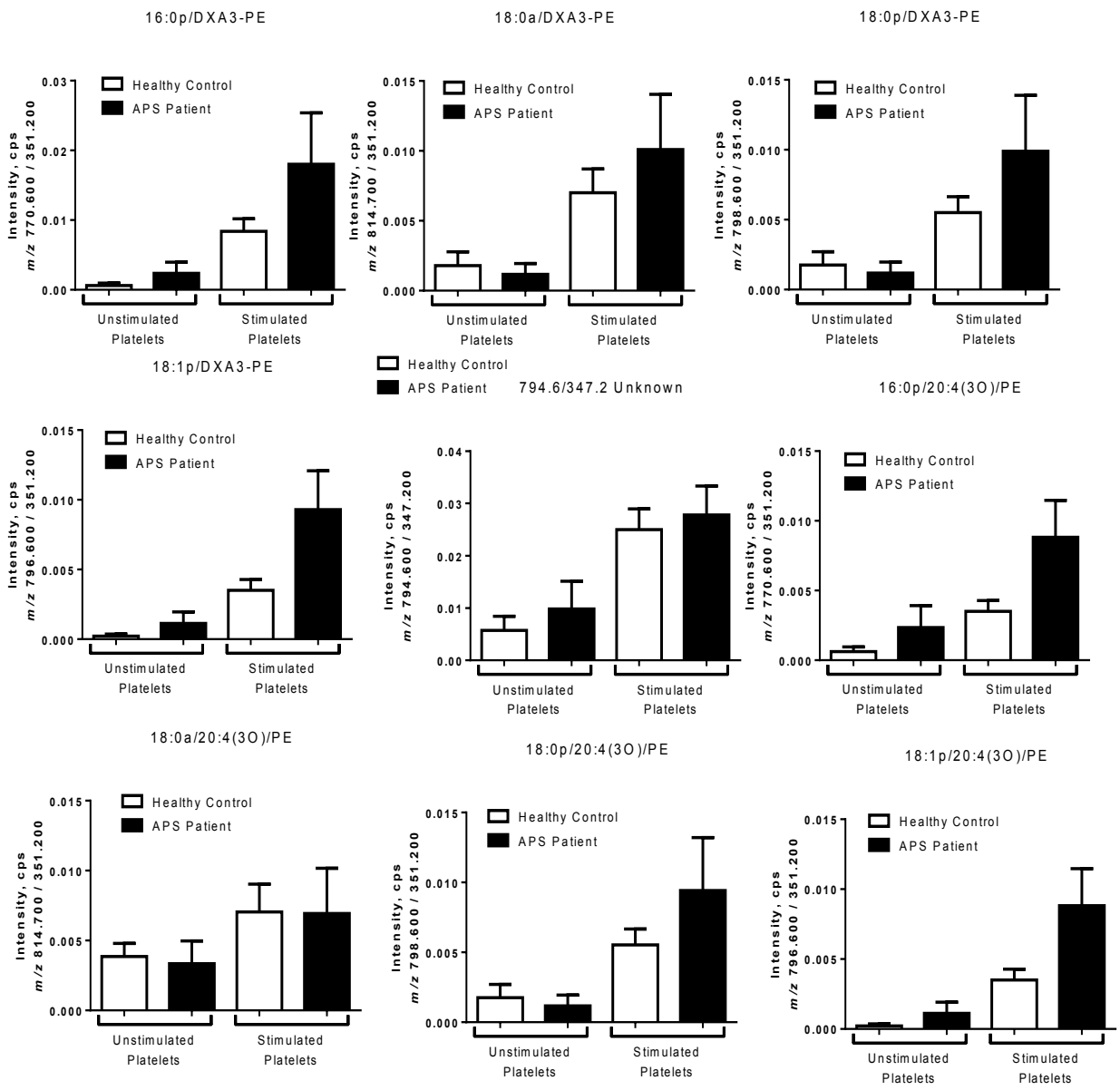
16:0p/DXA3-PE
18:0a/DXA3-PE
18:0p/DXA3-PE
Healthy Control
APS Patient
Intensity, cps
m/z 770.600 / 351.200
m/z 814.700 / 351.200
m/z 798.600 / 351.200
Unstimulated Platelets
Stimulated Platelets
18:1p/DXA3-PE
794.6/347.2 Unknown
16:0p/20:4(3O)/PE
m/z 796.600 / 351.200
m/z 794.600 / 347.200
18:0a/20:4(3O)/PE
18:0p/20:4(3O)/PE
18:1p/20:4(3O)/PE

fig. S3

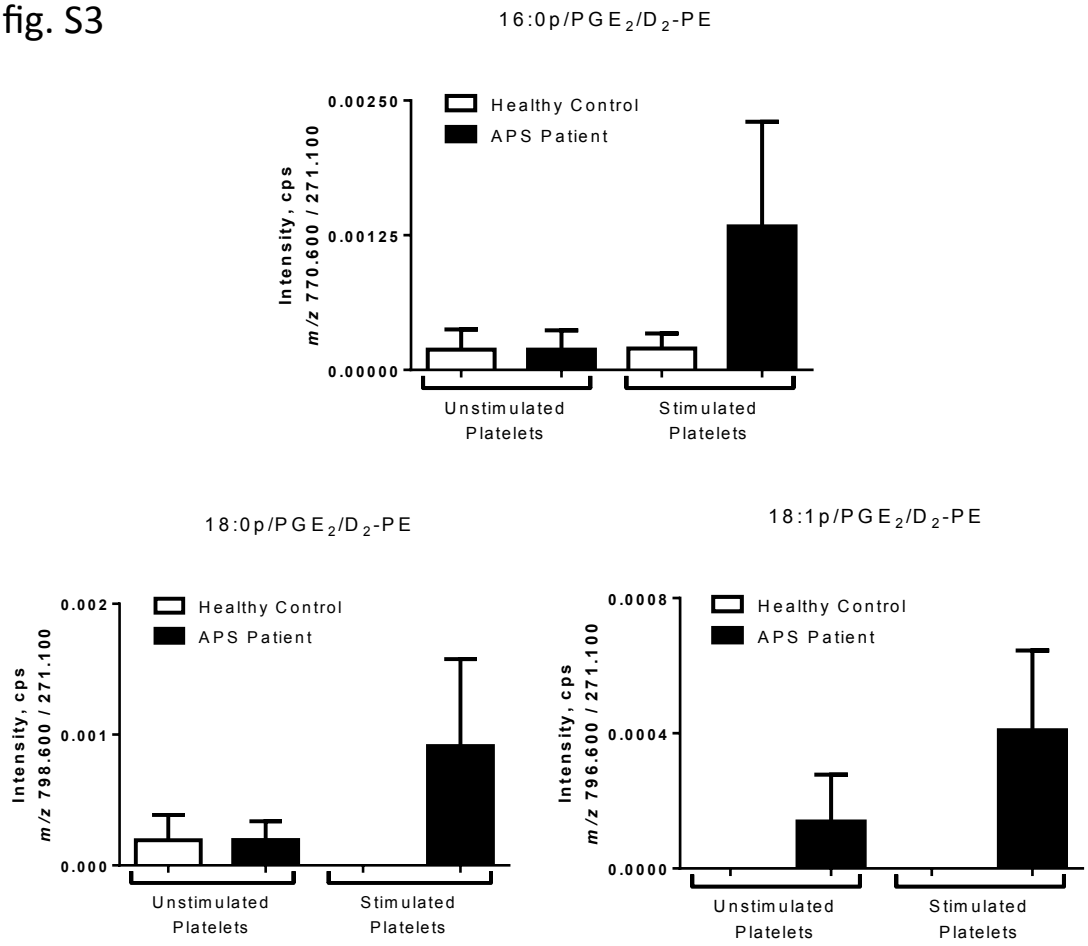

Figure S3. Primary data for generation of eoxPL by human washed platelets from HC and APS patients. Washed platelets were activated using thrombin as outlined in Methods then analyzed for eoxPL using LC/MS/MS. Levels are expressed relative to internal standard (DMPE/DMPC) (n=16 HC, n=10 APS, mean +/- SEM).

fig. S4 Correlation plot for patient samples

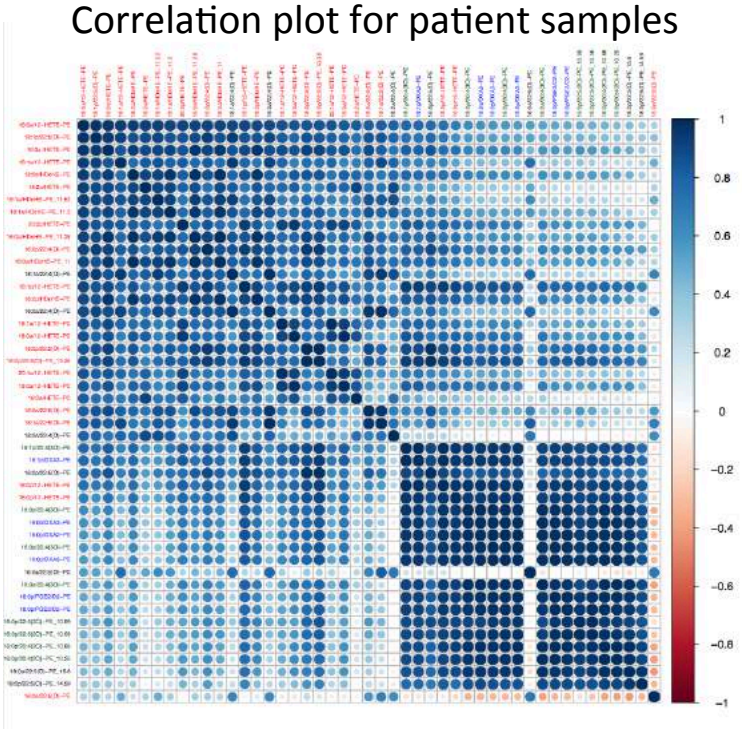

Correlation plot for healthy control samples

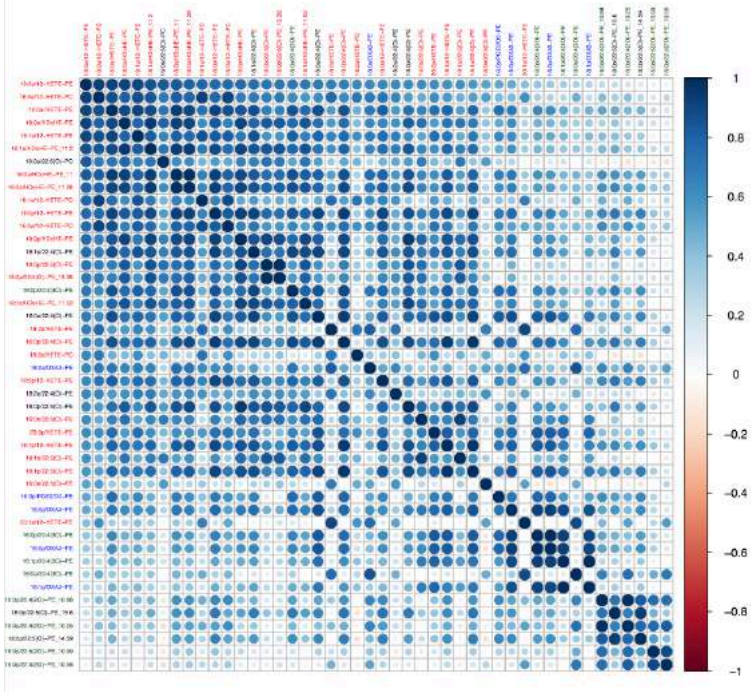

Figure S4. Correlation plots for lipids from either HC or APS groups shows that lipids group according to enzymatic origin. Correlations between lipids across the whole cohort were plotted in a grid, in order of decreasing correlation as described in Methods. Red: p12-LOX, blue: COX-1, green: polyoxygenated PL, black: unknown origin.

Figure S1. Primary data for generation of eoxPL by wild type and p12-LOX$^{-/-}$ washed platelets. Blood was taken by cardiac puncture and washed platelets isolated as in Methods. Platelets were activated using thrombin as outlined in Methods then analyzed for eoxPL using LC/MS/MS. Levels are expressed relative to internal standard (DMPE/DMPC) (n=3, mean +/- SEM).

Figure S2. Analysis of HC and APS demographics for effects on eoxPL generation shows no effect of age, gender or arterial thrombosis on platelet 12-HETE-PEs. Data was analysed for platelet 12-HETE-PEs, either unstimulated (US) or following thrombin treatment, versus (A) age, APS, (B) age, HC, (C, D) gender, (E) venous vs arterial thrombosis.

Figure S3. Primary data for generation of eoxPL by human washed platelets from HC and APS patients. Washed platelets were activated using thrombin as outlined in Methods then analyzed for eoxPL using LC/MS/MS. Levels are expressed relative to internal standard (DMPE/DMPC) (n=16 HC, n=10 APS, mean +/- SEM).

Figure S4. Correlation plots for lipids from either HC or APS groups shows that lipids group according to enzymatic origin. Correlations between lipids across the whole cohort were plotted in a grid, in order of decreasing correlation as described in Methods. Red: p12-LOX, blue: COX-1, green: polyoxygenated PL, black: unknown origin.